

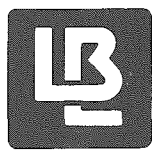
154
1-21-88
JB

4

Z-111

DR-0368-9

LBL-23096
UC-11



Lawrence Berkeley Laboratory

UNIVERSITY OF CALIFORNIA

EARTH SCIENCES DIVISION

A Borehole Fluid Conductivity Logging Method for the Determination of Fracture Inflow Parameters

C.-F. 3 a.

October 1987



DISCLAIMER

This report was prepared as an account of work sponsored by an agency of the United States Government. Neither the United States Government nor any agency Thereof, nor any of their employees, makes any warranty, express or implied, or assumes any legal liability or responsibility for the accuracy, completeness, or usefulness of any information, apparatus, product, or process disclosed, or represents that its use would not infringe privately owned rights. Reference herein to any specific commercial product, process, or service by trade name, trademark, manufacturer, or otherwise does not necessarily constitute or imply its endorsement, recommendation, or favoring by the United States Government or any agency thereof. The views and opinions of authors expressed herein do not necessarily state or reflect those of the United States Government or any agency thereof.

DISCLAIMER

Portions of this document may be illegible in electronic image products. Images are produced from the best available original document.

CONFIDENTIAL
UNCLASSIFIED
REVIEW

DISCLAIMER

This document was prepared as an account of work sponsored by the United States Government. Neither the United States Government nor any agency thereof, nor The Regents of the University of California, nor any of their employees, makes any warranty, express or implied, or assumes any legal liability or responsibility for the accuracy, completeness, or usefulness of any information, apparatus, product, or process disclosed, or represents that its use would not infringe privately owned rights. Reference herein to any specific commercial products process, or service by its trade name, trademark, manufacturer, or otherwise, does not necessarily constitute or imply its endorsement, recommendation, or favoring by the United States Government or any agency thereof, or The Regents of the University of California. The views and opinions of authors expressed herein do not necessarily state or reflect those of the United States Government or any agency thereof or The Regents of the University of California and shall not be used for advertising or product endorsement purposes.

Printed in the United States of America
Available from
National Technical Information Service
U.S. Department of Commerce
5285 Port Royal Road
Springfield, VA 22161
Price Code: A04

Lawrence Berkeley Laboratory is an equal opportunity employer.

DISCLAIMER

This report was prepared as an account of work sponsored by an agency of the United States Government. Neither the United States Government nor any agency thereof, nor any of their employees, makes any warranty, express or implied, or assumes any legal liability or responsibility for the accuracy, completeness, or usefulness of any information, apparatus, product, or process disclosed, or represents that its use would not infringe privately owned rights. Reference herein to any specific commercial product, process, or service by trade name, trademark, manufacturer, or otherwise does not necessarily constitute or imply its endorsement, recommendation, or favoring by the United States Government or any agency thereof. The views and opinions of authors expressed herein do not necessarily state or reflect those of the United States Government or any agency thereof.

LBL--23096

DE88 004883

A Borehole Fluid Conductivity Logging Method for the Determination of Fracture Inflow Parameters

Chin-Fu Tsang

Earth Sciences Division
Lawrence Berkeley Laboratory
University of California
Berkeley, California 94720

October 1987

10-1987
10-87

ef

Abstract

It is of much current interest to determine the flow characteristics of fractures intersecting a wellbore in order to provide data in the estimation of the hydrologic behavior of fractured rocks. In particular the fluid inflow rates from the fractures into the wellbore are important quantities to measure. However often these inflows are at very low rates. In addition very often one finds that only a few percent of the fractures identified by core inspection and geophysical logging are water-conducting fractures, the rest being closed, clogged or isolated from the water flow system. A new procedure is proposed and a corresponding method of analysis developed to locate water-conducting fractures and obtain fracture inflow parameters by means of a time sequence of electric conductivity logs of the borehole fluid. The physical basis of the analysis method is discussed. The procedure is applied to an existing set of data, which shows initiation and growth of nine conductivity peaks in a 900-m section of a 1690-m borehole, corresponding to nine water-conducting fractures intersecting the borehole. We are able to match all nine peaks and determine the flow rates from these fractures. Further experiments are suggested to validate this technique.

Introduction

In the study of the hydrology of fractured rocks, it is important to know the fracture properties. Surface observations may be useful, but the more relevant observations are those made at the depths of interest. Such measurements are mainly carried out through boreholes or underground openings. In the case of boreholes various methods of studying fracture properties have been used. For example, a downhole televiewer can be used to map the fracture traces on the borehole walls and determine their density and orientations. However, it is well known that often these traces do not correspond to locations of water-conducting fractures. Hence, there is a need to (1) identify the location and (2) measure directly the hydraulic or flow properties of an identified water-conducting fracture or group of fractures intersected by the borehole.

Constant-pressure, constant-flow or pulse tests have been applied to packed intervals along a wellbore. Since many of the fractured rocks of interest are of low permeability, the flow from a packed interval can be very slow. This has necessitated the development of low-flow measurement tools and the use of long-term measurements involving many packed intervals tested one at a time. Packed-off test intervals are usually larger than individual water-conducting zones, thus leading to an uncertainty in the location of a water-bearing fracture. An alternative method is the measurement of inflow along the borehole from fractures without the use of packers, with the well flowing at a moderate rate. Borehole flowmeters (see e.g., Hufschmied, 1983; Omega, 1987; Bean, 1971) can in principle yield the inflow rate from individual inflow zones. Such a flowmeter log is often strongly affected by wellbore radius variations. Thus, a caliper log has to be run to calibrate the results. Also, there is a low flow rate limit below which the conventional flowmeter log is no longer useful.

The present paper stems from a suggestion by Peter Hufschmied, Marc Thury and coworkers at Nationale Genossenschaft für die Lagerung radioaktiver

Abfälle (NAGRA), Baden, Switzerland. The method involves the use of a time sequence of electric conductivity logs of borehole fluid. The following section describes the logging procedure and the analysis method used. Next, analytic considerations are discussed to show the functional dependence and expected results for the short and long time limits. Then the numerical code used in the data analysis is introduced. A set of data from the NAGRA Leuggern borehole is then described and our analysis method applied to evaluate the inflow characteristics. Finally, further experiments are suggested for the validation of this technique.

Fluid Conductivity Logging Procedure

Consider the uncased section of a wellbore that intersects a number of flowing fractures. In general, the flowing fractures contain fluids with different chemical compositions and ion content, and hence different electric conductivities. The relationship between ion concentration and fluid electric conductivity is reviewed, for example, by Shedlovsky and Shedlovsky (1971), who give graphs and tables relating these two quantities. Hale and Tsang (1987) made a sample fit for the case of NaCl solution at low concentrations and obtained

$$\sigma = 0.187C - 0.001C^2$$

where σ is the fluid electric conductivity in S/m and C is concentration of NaCl in kg/m^3 . The formula is valid at a temperature of 20 °C, and for values of C up to $\approx 6 \text{ kg/m}^3$ and values of σ up to 1.1 S/m (or 11000 $\mu\text{S/cm}$). The quadratic term can be dropped if one is interested only in values of C up to $\approx 4 \text{ kg/m}^3$ and σ up to 0.8 S/m (or 8000 $\mu\text{S/cm}$). In this case we have a convenient linear relationship between σ and C :

$$\sigma(\mu\text{S/cm}) = \alpha C(\text{kg/m}^3) \tag{1}$$

where $\alpha = 1870 (\mu\text{S/cm}) \cdot (\text{m}^3/\text{kg})$ and the units were chosen because in applications described later in the paper σ is given in $\mu\text{S/cm}$.

Suppose the wellbore is first washed out with de-ionized water by passing a tube to the well bottom. There will be some residual ion content and associated electric conductivity. In the field data shown later in the paper, the residual electric conductivity turns out to be about $60 \mu\text{S}/\text{cm}$, corresponding to a residual salinity concentration of $0.03 \text{ kg}/\text{m}^3$. Now let us produce from the wellbore at a flow rate Q . For three fractures we have a situation shown schematically in Figure 1. Note that the flow rates at different parts of the wellbore are different, being equal to the sum of all upstream inflow rates. At each fracture inflow point, the parameters characterizing the flow are t_{oi} , the time when the fracture fluid emerges at the wellbore; x_i , the location of the inflow point; q_i , the volumetric inflow rate; and $q_i C_{oi}$, the solute mass inflow rate, where C_{oi} is the concentration of ionic solutes in the fracture fluid. Here we have assumed that generally t_{oi} can be different for different fracture inflow points. This could be due to different initial hydraulic heads in these fractures or the specific borehole development and pressure history.

Figures 2-5 display schematically salinity distribution inferred from fluid electric conductivity distribution in the wellbore for a series of times. Figure 2 shows the curves for early values of time. In this paper we assume that the wellbore cross section is small compared with its length, so that salinity or chemical concentration is uniform at each cross section. If there is no overall vertical upward flow in the wellbore and density effects can be neglected, one expects the salinity curves at each inflow point to be symmetrical about the inflow point (see formula in the next section). When the well is pumped at a given flow rate, a skewing of the curves is expected due to the upward flow in the wellbore, which is larger near the well top than near the well bottom.

Figures 3-5 show three possible sets of salinity curves for large time periods, all assuming very small borehole diffusivity. Figure 3 shows one possible set of results. At large times, the saturation salinity is given by

$$C_{\max,1} = \frac{wC_w + q_1 C_1}{w + \sum_{n=1}^1 q_n} \quad (2a)$$

where q_i is the inflow rate, with $i = 1$ corresponding to the deepest inflow point (i.e., most upstream), and w is the borehole flow rate from well-bottom with salinity, C_w . If the salinity curves from two inflow points i and $i + 1$ overlap, then $C_{\max,i}$ is still given by (1), but $C_{\max,i+1}$ is given by

$$C_{\max,i+1} = \frac{wC_w + q_i C_i + q_{i+1} C_{i+1}}{w + \sum_{n=1}^{i+1} q_n} \quad (2b)$$

There is a step-jump at the location of the $(i+1)$ -th inflow point when the salinity curve from i -th inflow reaches the $(i+1)$ -th location. This is demonstrated in Figure 3 for three inflow points, with second and third inflow salinity curves interfering with each other.

At the limit of very large time periods, the expected salinity curves are shown in Figure 4. Here the step structure is prominent, with the C_{\max} value between the i -th and $(i+1)$ -th inflow points given by

$$C_{\max,i} = \frac{wC_w + \sum_{n=1}^i q_n C_n}{w + \sum_{n=1}^i q_n} \quad (3)$$

With diffusion, the step structure will be smeared out. Note that the results, equations (2) and (3), are independent of variations of wellbore radius.

Figure 5 shows a sequence of curves from early to later times. In this figure, the effect of having one of the three inflows starting much earlier than the other two is shown.

Thus, the procedure for fluid conductivity logging is as follows. After the wellbore fluid is replaced by de-ionized water, the well is produced at a low flow rate. Then a fluid conductivity logging probe is run through the well-bore and electric conductivity distribution recorded at several times. Care should be taken not to disturb the wellbore fluid to induce large scale disturbances. With the time sequence of fluid conductivity logs, the inflow characteristics of the fractures

can then be determined. For the field case described later in the paper, the well is about 1690 m deep with the section under survey ranging from 770 to 1637 m below the surface. Each logging run took about an hour and five logs were taken at intervals of about 4 to 20 hours.

Analytic Considerations

In this section three simple analytic solutions are described. They illustrate key issues encountered in carrying out the flow conductivity logging and analysis.

For the flow in the wellbore to be below the turbulence regime, the Reynold's number, R , is below the critical value of about 2000. It is well known (e. g., Roberson and Crowe, 1985) that for a wellbore

$$R = \frac{vd}{\nu} \quad (4)$$

where v is linear velocity in the wellbore, d is wellbore diameter and ν the kinematic viscosity of the fluid. For example, if the well diameter is $d = 15$ cm and wellbore flow rate is 10 l/min, implying a linear flow velocity of about 10^{-2} m/sec, the Reynold's number is about 1500 for room-temperature water. This is below the critical Reynold's number.

For early times, the salinity concentration is still localized near the inflow points, so that we may consider each inflow point by itself. Further, if we assume that the overall wellbore flow velocity is relatively small and has little effect on the salinity curves at these early times, the problem is then equivalent to release of a chemical beginning at time, $t = 0$, at a given point, $x = 0$, say, in a linear pipe of stationary water, and an analytic solution is available. An important parameter here is D , the molecular diffusion parameter associated with the spread of the chemical after it enters the pipe. If the mass inflow rate is qC_o , where q is flow rate in m^3/s and C_o is concentration of inflow fluid in kg/m^3 , and d is wellbore diameter in meters, the solution is given by (see e.g., Fischer et al., 1979).

$$C(x,t) = \frac{qC_o}{\sqrt{4\pi D}} \cdot \frac{4}{\pi d^2} \cdot \int_0^t \frac{1}{\sqrt{t-\tau}} \exp\left(-\frac{x^2}{4D(t-\tau)}\right) d\tau \quad (5)$$

A plot of this is shown in Figure 6. Several interesting properties of this expression that will be useful later are pointed out here. First, at the inflow point, $x = 0$, we find the following expression for peak height:

$$C(0,t) = \frac{qC_o}{\sqrt{\pi D}} \cdot \frac{4}{\pi d^2} \cdot \sqrt{t}$$

so that

$$[C(0,t)]^2 = \frac{(qC_o)^2}{\pi D} \cdot \frac{16}{\pi^2 d^4} \cdot t \quad (6)$$

This shows that $[C(0,t)]^2$ is linearly dependent on t for early times and the slope of $[C(0,t)]^2$ versus t is $S_c = 16(qC_o)^2/\pi^3 D d^4$. If the release of chemicals at the wellbore begins at $t = t_o$, the formula can be easily modified to show that a plot of $[C(0,t)]^2$ versus t should have an x-intercept at t_o . Ideally, t_o for all the inflow points should be the same, equal to the time when pumping starts. However they can be different if the fractures are at different initial hydraulic potentials relative to the wellbore, or if there are operational problems in pumping de-ionized water into the wellbore to establish initial conditions. Furthermore, if we calculate the area under the salinity curves at these early times, we obtain

$$\int C(x,t) dx = (qC_o) \cdot \frac{4}{\pi d^2} \cdot t \quad (7)$$

as one would intuitively expect. Now a plot of $\int C(x,t) dx$ versus t will give a slope of $S_A = 4qC_o/\pi d^2$. Then, the ratio S_A^2/S_c is just πD , a constant. The validity of the early time data can be checked by comparing this ratio for a number of inflow points in the same wellbore. Thus, by these simple considerations, one can obtain from early time curves both t_o and (qC_o) .

In principle, once t_o and qC_o are obtained for each peak, one can apply large-time results, equations (1)-(3), to calculate the flow rate of the particular inflow point. Thus, from careful measurements of early-time log data and late-

time log data, one can obtain all the inflow flow rates in a simple and straightforward way. These results are not sensitive to moderate variations of wellbore diffusivity. Note also that while the short-term results depend on wellbore radius, the large-time results (equations 1-3) are independent of it.

Another analytic solution is available for the case where the inflow is well established and the wellbore flow dominates the movements of the inflow salinity. This corresponds to the problem of a continuous inflow at constant qC_o at $x = 0$. Here

$$K \frac{\partial^2 C}{\partial x^2} - v \frac{\partial C}{\partial x} = \frac{\partial C}{\partial t} \quad (8)$$

with

$$C(x,t) = 0 \quad \text{at } t = 0$$

$$\frac{\partial C}{\partial x} = 0 \quad \text{at } x = \infty$$

and

$$C(0,t) = C_o \quad \text{for } t > 0$$

In these equations v is the linear velocity given by q divided by the wellbore cross section area, and K is the asymptotic mechanical dispersion coefficient in a linear pipe, which is well studied by Taylor (1953), Aris (1956) and others. These authors found

$$K = \frac{d^2 v^2}{192D} \quad (9)$$

where d is the wellbore diameter, v is the linear flow velocity and D is the molecular diffusivity. Note that the boundary condition $C(0,t) = C_o$ for $t > 0$ in the constant linear flow stream with velocity v implies a constant solute release of vC_o at $x = 0$. However not all solute flows up the borehole; there is a small amount ($K\partial C/\partial x$) that is diffused down the borehole (see equation (8) and Javandel et al. 1984).

The solution of the above differential equation (see e.g., Ogata and Banks, 1961) is

$$\frac{C}{C_o} = \frac{1}{2} \operatorname{erfc} \left[\frac{x-vt}{2\sqrt{Kt}} \right] + \frac{1}{2} \exp \left(\frac{vx}{K} \right) \operatorname{erfc} \left[\frac{x+vt}{2\sqrt{Kt}} \right] \quad (10)$$

A plot of this solution is shown in Figure 7. One sees the steady migration of the salinity curves downstream, eventually saturating the whole wellbore with fluid of concentration C_o .

Numerical Method

For a general problem of multiple inflow points, overlapping salinity curves and variable dispersion coefficient K , no analytic solution is readily available and numerical methods are required. For our purpose, we developed a simple computer code (Hale and Tsang, 1987) that solves the linear advective-dispersive equation:

$$K \frac{\partial^2 C}{\partial x^2} - v \frac{\partial C}{\partial x} + S = \frac{\partial C}{\partial t}$$

where C is the concentration of solute, K is the dispersion coefficient, v is the linear borehole fluid velocity, and S is the source term, under the initial condition:

$$C(x,0) = C_o(x) \quad x \leq x_{\max}, t = 0.$$

Here x_{\max} represents the deepest point of interest in the borehole. The code uses a finite difference solution scheme with upstream weighting and can accommodate various boundary conditions. It has been verified against a number of analytic solutions and also against a well-validated numerical code, PT (Bodvarsson, 1982; Tsang 1985; Tsang and Doughty, 1985). It is available on PC-diskette (Hale and Tsang, 1987).

In this section we shall present a few results of fluid salinity behavior in the wellbore to confirm the earlier schematic and analytic considerations and to study

parameter sensitivities. In the next section on field experiments and data, we shall apply the code with actual parameters to analyze the data and evaluate the inflow parameters.

Figure 8 shows the numerical results of a case with one inflow point under an overall inflow flow rate w . It is apparent that at early times, the salinity peak grows in a way similar to the early time analytic solution given by equation (5) (Figure 6). At later times, after the salinity value saturates to the inflow fluid salinity, the behavior is similar to that given by the late-time analytic solution, equation (10) (Fig. 7).

Figure 9 shows a late-time numerical solution for the case of the overall wellbore fluid flow rate w equal to 0, $q/3$ or q , where q is the fracture inflow rate. The saturation salinity values are C_o , $3/4 C_o$ and $1/2 C_o$ respectively. This is obvious from the proportionate mixing of inflow salinity with the upcoming wellbore flow with $C_w = 0$ (equation 1). Note that we are using the volume flow rates w and q and not linear velocities. Thus, the variation of wellbore cross-section has no effect on these results.

Figures 10a and 10b show the salinity curves in the wellbore for two different values of wellbore dispersivity, K . Here we assume that $w = 0$. Because there is a closed boundary at well bottom $x = 0$, there is still a preferred flow upwards to $-x$ values. With inflow at rate q at the point $x = -50$ m, the flow rate in the wellbore is q downstream from $x = -50$ m and 0 upstream. In Figure 10a the value of K is $6.25 \times 10^{-6} \text{ m}^2/\text{s}$, and in Figure 10b it is doubled. The curves display only small differences from each other, indicating low sensitivity to moderate uncertainties in K values.

Figures 11-13 show the interference between two inflow points. In all of these cases K is taken to be $1.25 \times 10^{-5} \text{ m}^2/\text{s}$ and the overall wellbore flow rate to be $w = 1.5 \times 10^{-7} \text{ m}^3/\text{s}$. The two inflow points are at $x = -50$ m and $x = -100$ m with flow rates $q_1 = 1.5 \times 10^{-7} \text{ m}^3/\text{s}$ and $q_2 = 3 \times 10^{-7} \text{ m}^3/\text{s}$ respectively (Figure 11). Interference effects are seen when the salinity curve from the upstream

inflow point overlaps the downstream point. Interference is drastically increased if the upstream inflow rate q_1 is doubled to $q_1 = 3 \times 10^{-7} \text{ m}^3/\text{s}$ (Figure 12). Figure 13 shows the large time period results with the upstream inflow (at $x = -50 \text{ m}$) arbitrarily assumed to have a later starting time than the downstream inflow point (at $x = -100 \text{ m}$). The step structure at large times confirms that shown in Figure 4.

Field Experiment and Data Analysis

Fluid logging experiments were carried out by Nationale Genossenschaft für die Lagerung radioaktiver Abfälle (NAGRA) of Switzerland in different boreholes during 1985. A brief overview of the overall testing program and results is given by Thury and Gautschi (1986). Measurements from the Leuggern borehole are taken as an example to demonstrate the applicability of the method. The Leuggern borehole extends 1689 m into crystalline bedrock. It was cased from the ground surface to a depth of 267 m, and a production-injection packer was set at 1637 m to shut off a highly permeable section near the bottom of the borehole. This was necessary to avoid a high flow rate through the low-permeability section, which would have covered up the very small inflow from this section. Only the section between 770 m and 1637 m was studied by the fluid log measurements. First the borehole water was replaced by de-ionized water through a downhole tubing, and the fluid conductivity was measured at the outflow at welltop to be $60 \mu\text{S}/\text{cm}$. Then the tubing was pulled out of the well and the water level in the well was kept at zero by pouring de-ionized water into it. A pump was placed at -210 m, and background temperature and electric conductivity logs were taken. Then with pumping maintained at about 20 l/min a series of 5 complete electric conductivity logs were taken over two days. After that a temperature log was again taken.

The conductivity logs are shown in Figures 14 and 15. Figure 14 shows only the upper portion of the section studied (700-1000 m), displaying two inflow points; Figure 15 shows the full section displaying nine major inflow points. For

the sake of discussion, these peaks are labeled 1 through 9, as shown in these figures. The wellbore diameter over the section is 5 1/2 inches or 14 cm. The temperature log shows an increase of temperature with depth that can be approximated adequately by

$$T = 10 + \frac{x}{30} \quad (11)$$

where x is in meters and T in $^{\circ}\text{C}$. The fluid electric conductivity, σ , depends on temperature. In order to convert the measured values shown in Figures 14 and 15 to normalized conductivity values at a uniform temperature, T_n , of 20°C , the following formula (NAGRA, 1987) is used:

$$\sigma(T_n) = \frac{\sigma(T)}{1 + 0.022(T-20)} \quad (12)$$

The field data are digitized and then normalized according to equations (11) and (12). The normalized electric conductivity log is shown in Figure 16. Now we proceed to study and match the nine peaks in this figure.

First let us calculate the Reynold's number, R , for flow in this case. By equation (1) we see $R = vd/\nu$. For well head pumping rate $Q = 20 \text{ l/min}$, wellbore diameter is $d = 14 \text{ cm}$, and ν is given by water kinematic viscosities at the appropriate temperatures ($0.3 - 1 \times 10^{-6} \text{ m}^2/\text{s}$), the Reynold's number at the well head is $R \approx 3000$. This is above the critical value and the flow is in the laminar-turbulent transition region. If $Q = 2 \text{ l/min}$, then $R \approx 300$, much smaller than the critical Reynolds number of 2000.

The positions of the nine peaks range from the deepest one (peak 1) at $x = 1440 \text{ m}$ to the most shallow one (peak 9) at $x = 843 \text{ m}$. We have selected an arbitrary starting time of pumping as a reference. Peaks 8 and 9 have data at 13.03 hours relative to this reference time. All peaks have data at 27.12, 31.28, 38.41 and 57.24 hours. We consider the starting times of these inflows to be unknown and possibly different from each other. First let us treat these peaks independently and apply the results from equations (5) - (7), where we convert the concentration C to conductivity values σ by means of equation (1).

Figure 17 shows the plots of $[\sigma(0,t)]^2$ versus time t . We assume that only the data at the earliest two to three times satisfy the early time requirements of equation (5). Then a line joining these early time values yields the slope and intercept, which corresponds to $S_c = 16(\alpha q C_o)^2 / \pi^3 D d^4$ and t_o for each peak respectively. These values are listed in Table 1. Figure 18 shows the plot of $\int \sigma(x,t) dx$ versus time t . Again, the slopes and intercepts of the early times are found and listed in Table 2. It is noted that the t_o values found for each peak from these two methods do not agree with each other. This may be due to numerical difficulties in determining the peak value and the area under each of the curves and the assumptions underlying equation (5). For the case of peak 9, the data are incomplete at the lower x values and, for peak 4, the $\sigma(0,t)$ value is hard to determine because of the overlap of neighboring curves. An interesting result is the ratio, S_A^2/S_c , of the slopes obtained for each peak. As explained in an earlier section, this should be equal to πD , a constant for all the peaks. The results of Table 2 show that, omitting peak-4 and peak-9 data, the values are within a factor of two of each other, with a mean value of $\overline{\pi D} = 24.8 \text{ m}^2/\text{hr}$ or $7 \times 10^{-3} \text{ m}^2/\text{s}$. This is much larger than would be expected for molecular diffusion which typically yields a value for $D_m \approx 10^{-8} \text{ m}^2/\text{s}$. The larger value for $\overline{\pi D}$ in our problem, we believe, is due to dilution effect during the initial inflow of high-salinity water into the borehole cross-section of finite radius. If the borehole radius were zero or negligible, diffusion would just occur along the length of the well, which is the case described by our early-time analytic solution. Since the borehole has finite radius, the dilution of incoming saline water within the cross-section results in a large effective diffusion coefficient. For advection-dispersion calculations of saline water up the wellbore, the smaller D_m value may be the more appropriate one to use.

Having made the above analysis, we proceed to apply the numerical code described in the last section to match all nine peaks and attempt to obtain the parameters t_{oi} , q_i and C_{oi} . First we need initial guesses for these parameters, which are obtained as follows. For each peak, we can easily determine its

location, x_i , by inspection of Figure 16. The quantity $q_i C_{oi}$ can be obtained in two ways. The first is to use the value of S_c from Table 1 and the mean value of $\overline{\pi D}$ to calculate:

$$q_i C_{oi} = \sqrt{S_c(\overline{\pi D})} \cdot (\pi d^2/4)/\alpha \quad (13)$$

The other way is to use S_A from Table 2 directly and solve for $q_i C_{oi}$ by:

$$S_A = 4\alpha q_i C_{oi}/\pi d^2 \quad (14)$$

In principle, the values of the parameters, t_{oi} and $q_i C_{oi}$, obtained from Tables 1 and 2 should be the same if the early time requirement is satisfied. The present data set does not give equal parameter values, because insufficient data were obtained in the first 10-15 hours. The uncertainties are particularly large for the highest two peaks, peaks 9 and 8, which carry most of the flow. Also, the borehole diameter, d , may not be constant along the length of the borehole. Hence, in choosing the parameter values we have considered both Table 1 and Table 2 in a complementary way and have come up with a set of initial guesses. Then, these are adjusted to obtain parameters for the numerical code that yield the best match to observed data.

The primary parameter to be determined is q_i , the value of the flow rate for each inflow point. Since we do not have data corresponding to large-time limit data in order to use equations (1) - (3), these have to be found by successive guesses, under the constraint that

$$\Sigma q_i = Q.$$

if Q can be measured independently. For the present data set, the value of Q is uncertain (see below).

The wellbore dispersivity parameter, K , is given by equation (9), where $d = 14$ cm, and q and D will be estimated as follows. Anticipating the results of data-matching discussed below, q for the whole section of the borehole under study ($\approx 770 - 1637$ m) is about 2 l/min. However the highest two inflow points at 843 m and 918 m represent 80% of the total flow. So the approximate mean

flow rate over the remainder of the borehole section is assumed to be 0.2 l/min. Based on the discussions above, we decide that it is inappropriate to use a value of D derived from $\overline{\pi D} = 7 \times 10^{-3} \text{ m}^2/\text{s}$, because of the borehole cross-section dilution effect. Instead, we assume that $D = D_m \approx 10^{-8} \text{ m}^2/\text{s}$. Using these parameters, we find that $K = 5 \times 10^{-4} \text{ m}^2/\text{s}$. This is used as the initial guess value. Slight adjustment can then be made on K to optimize the data match.

A number of attempts of data matching are made, some of which are shown below. Table 3 shows the parameters for one of our first attempts. In this table, $q_i C_{oi}$ are obtained using equation (14). The values of q_i are assumed to be proportional to $q_i C_{oi}$ and, based on earlier information we received should add up to $Q = 3.3 \times 10^{-4} \text{ m}^3/\text{s}$ ($\approx 20 \text{ l/min}$). The results are shown in Figure 19. It is apparent from this figure that all the peaks are much lower than the observed data (Figure 16). A few further attempts show us that it is impossible to match the data with this assumed value of Q . By adjusting Q , we found that we can match the data if $Q \approx 2 \text{ l/min}$, ten times less than the number we used originally. We then sent a request to NAGRA (1987), who went back to the field data and found that the value of flow rate from the field experiment may be dominated by flow from a wellbore section above the section under study. The value of Q may indeed be only $3.3 \times 10^{-5} \text{ m}^3/\text{s}$ or 2 l/min . This is used for all later calculations.

Table 4 gives the parameters for the base case used for the sensitivity studies. These are the same as Table 3 except all the q_i values are reduced by a factor of 2 and hence C_{oi} values are increased by a factor of 2 in order to keep $q_i C_{oi}$ constant. The results are shown in Figure 20. Now the key parameters are varied to display the sensitivity of the peaks to these variations. Figure 21 shows the results when the dispersion coefficient is changed from $5 \times 10^{-4} \text{ m}^2/\text{s}$ to $5 \times 10^{-5} \text{ m}^2/\text{s}$. The results are relatively insensitive. Figure 22 shows the results based on parameters given in Table 4 except that q_i are all reduced by a factor of 2, and C_{oi} increased by a factor of 2, while keeping $q_i C_{oi}$ constant. Figure 23

shows the results based on parameters given in Table 4 except that q_1 are increased by a factor of 2 and C_{oi} are decreased by a factor of 2, while keeping $q_1 C_{oi}$ constant. The dependence on these variations are quite instructive. The next two sets of calculations are made by reducing all $q_1 C_{oi}$ by a factor of 2 relative to the base case. This may be done by either decreasing q_1 by a factor of 2, or by decreasing C_{oi} by a factor of 2, with the results displayed in Figures 24 and 25 respectively.

After these sensitivity studies, the parameters for each peak are varied to obtain a best fit to observed data (Figure 16). The best fit was obtained by visually comparing calculated and observed curves. The results are shown in Figures 26 with the final matching parameters listed in Table 5. Figure 27 displays both the matching results and the observed data for the time = 57.24 hrs.

We next extrapolate the results to future times assuming the parameters in Table 5. The results shown in Figure 28 are the predicted results if the experiment were to be continued for a longer period of time.

Conclusion and Proposal for Further Validation Experiments

In this paper we first discussed the procedure and physical processes associated with a time series of fluid conductivity logs in a borehole intersected by a number of flowing fractures. Simple formulas to evaluate some of the relevant parameters are described and their uses demonstrated. Then numerical matching of the data to obtain the remaining parameters is shown. The results are not sensitive to borehole radius variations and the method may be able to measure small inflow rates. From Table 4, it appears that flow rates as low as $0.2 \times 10^{-6} \text{m}^3/\text{s}$ or $0.01 \text{ l}/\text{min}$ can be measured. This may prove to be a useful technique and may complement existing flow-meter or temperature-log methods.

To further validate the proposed method, we suggest that further experiments be performed in a borehole. The basic measurements are those described above for the field experiment by NAGRA. However the following additional

variations should be carried out. First, more than one value of the total flow rate, Q , should be used. Changing total flow rate will also change the individual inflow rates, q_i , and affect the skewness of the peaks.

Longer measurement times should be used. In the NAGRA case, increasing observation times to one or two weeks would probably allow some of the peaks to reach saturation and a flat salinity curve region to develop for some inflow points (see Figure 4). Such a flat region makes analysis more straightforward and less ambiguous.

More careful measurements of the early time data are important because we depend on them to determine some of the parameters.

Finally, the different saturating salinity values at the inflow points, C_{oi} , should be measured to validate the results obtained from our analysis.

Acknowledgements

Discussions and cooperation with NAGRA personnel, especially P. Hufschmied, M. Thury, A. Zingg, and P. Zuidema are much appreciated. Assistance in computation and graphing from C. Doughty and F. Hale are gratefully acknowledged. I would also like to thank C. Doughty, N. Goldstein, P. Hufschmied and I. Javandel for reviewing and commenting on the manuscript. The work is jointly supported by Nationale Genossenschaft für die Lagerung radioaktiver Abfälle, Switzerland; Engineering and Geoscience Division, Office of Basic Energy Sciences; and Repository Technology Division, Office of Civilian Radioactive Waste Management, U. S. Department of Energy through Contract No. DE-AC03-76SF00098.

References

- Aris, R. (1956), On the dispersion of a solute in a fluid flowing through a tube, *Proc. R. Soc. London, Series A* 235, 67-77.
- Bean, H. S. (1971), *Fluid meters: Their theory and application*, American Association of Mechanical Engineers, 6th Edition, New York.
- Bodvarsson, G. S. (1982), Mathematical modeling of the behavior of geothermal systems under exploitation, Ph.D. Thesis, University of California at Berkeley, Department of Materials Sciences and Mineral Engineering.
- Fischer, H. B., E. J. List, R. C. Y. Koh, J. Imberger, N. H. Brooks (1979), *Mixing in Inland and Coastal Waters*. Academic Press, New York.
- Hale, F. V. and C. F. Tsang, LBL-Report, in preparation for completion, September 1987.
- Hufschmied, P. (1983), Ermittlung der Durchlässigkeit von Lockergesteins - Grundwasserleitern, eine vergleichende Untersuchung verschiedener Feldmethoden, Diss. No. 7397, ETH Zurich, Switzerland.
- Javandel, I., C. Doughty and C. F. Tsang (1984), *Groundwater Transport*, Water Resources Monograph No. 10, American Geophysical Union, Washington, D. C.
- NAGRA (1987), Private Communication from Dr. Peter Hufschmied, NAGRA, Baden, Switzerland.
- Ogata, A. and R. B. Banks (1961), A solution of the differential equation of longitudinal dispersion in porous media, U. S. Geological Survey Prof. Pap. 411A, 34 pp.
- Omega (1987), *Complete Flow and Level Measurement Handbook and Encyclopedia*, Omega Engineering, Inc., Stamford, Connecticut.
- Roberson, J. A. and C. T. Crowe (1985), *Engineering Fluid Mechanics*, Houghton Mifflin Publishing Company, Boston, Massachusetts.

- Shedlovsky, T., and L. Shedlovsky (1971), "Conductometry," *Techniques of Chemistry*, (Arnold Weissberger and Bryant W. Rossiter, eds.), Vol. 1. Physical Methods of Chemistry, Part IIa, Electrochemical Methods, John Wiley & Sons, Inc., New York.
- Taylor, G. I. (1953), Dispersion of solute matter in solvent flowing slowly through a tube, *Proc. R. Soc. London*, Series A 219, 186-203.
- Thury, M., and A. Gautschi (1986), Testing programme in deep boreholes drilled in sediment-covered crystalline rocks in northern Switzerland, *Proceedings of the 2nd International Conference on Radioactive Waste Management*, September 7-11, 1986, Winnipeg, Manitoba, Canada.
- Tsang, C. F. (1985), Lessons learned in the verification and validation studies of a coupled heat and fluid flow code, Invited Paper. Proceedings of Symposium on Groundwater Flow and Transport Modeling for Performance Assessment of Deep Geologic Disposal of Radioactive Waste: A Critical Evaluation of the State of the Art, May 20-21, 1985, Albuquerque, New Mexico.
- Tsang, C. F. and C. Doughty (1985), Detailed validation of a liquid and heat flow code against field performance, Proceedings of the Eighth SPE Symposium on Reservoir Simulation, February 10-13, 1985, Dallas, Texas, organized by Society of Petroleum Engineers, Richardson, Texas.

**Tables
and
Figures**

Table 1. Data from $[\sigma(0,t)]^2$ vs t curves.

Peak No.	x (meters)	t_{oi} (hours)	S_c (μS) ² /cm ² hr
1	1440	18	929
2	1300	16	339
3	1215	19	711
4	1200	21	(854)
5	1188	19	892
6	1085	17	73
7	1048	2	402
8	918	9	55663
9	843	-24	34310

Table 2. Data from $\int_{-\infty}^{\infty} \sigma(x,t) dx$ vs t curves.

Peak No.	x (meters)	t_{oi} (hours)	S_A (100 μ S/hr)	S_A^2/S_c (m^2/hr)
1	1440	6	145	22.6
2	1300	3	102	30.7
3	1215	11	111	17.3
4	1200	13	47	(2.59)
5	1188	13	121	16.4
6	1085	11	40	21.9
7	1048	8	118	34.6
8	918	6	1243	27.8
9	843	6	(5449)	(866)

Table 3. Parameters used in initial match of field data

Peak No.	x (meters)	t_{oi} (hours)	$q_i C_{oi}$ (10^{-6}kg/s)	q_i ($10^{-6} \text{m}^3/\text{s}$)	C_{oi} (kg/m^3)
1	1440	18	0.33	6.5	0.051
2	1300	18	0.23	4.6	0.051
3	1215	18	0.26	5.0	0.051
4	1200	18	0.11	2.1	0.051
5	1188	18	0.28	5.4	0.051
6	1085	18	0.09	1.8	0.051
7	1048	2	0.27	5.3	0.051
8	918	9	2.9	56	0.051
9	843	-24	13	240	0.051
$K = 5.0 \times 10^{-4} \text{ m}^2/\text{s}$ $Q = 3.3 \times 10^{-4} \text{ m}^3/\text{s}$					

**Table 4. Parameters used in sensitivity analysis:
Base Case**

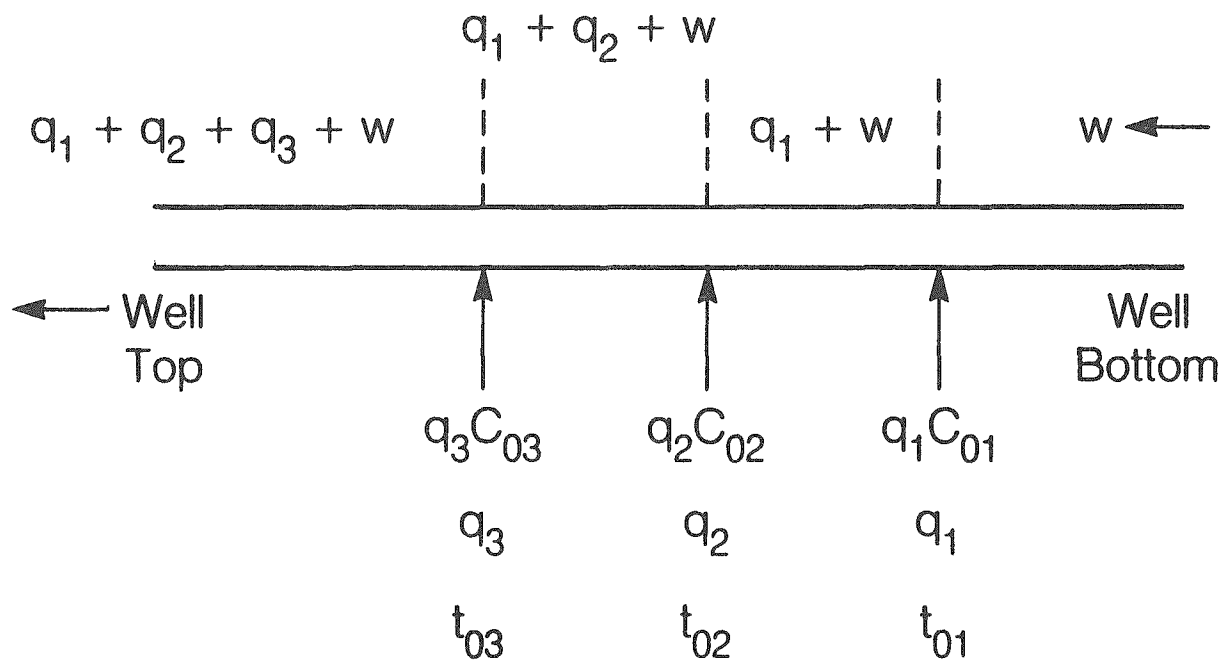
Peak No.	x (meters)	t _{oi} (hours)	q _i C _{oi} (10 ⁻⁶ kg/s)	q _i (10 ⁻⁶ m ³ /s)	C _{oi} (kg/m ³)
1	1440	18	0.33	0.65	0.51
2	1300	18	0.23	0.46	0.51
3	1215	18	0.26	0.50	0.51
4	1200	18	0.11	0.21	0.51
5	1188	18	0.28	0.54	0.51
6	1085	18	0.09	0.18	0.51
7	1048	2	0.27	0.53	0.51
8	918	9	2.9	5.6	0.51
9	843	-24	13.	24.	0.51

K = 5.0 x 10⁻⁴ m²/s
Q = 3.3 x 10⁻⁵ m³/s

Table 5. Parameters used in final match of field data.

Peak No.	x (meters)	t _{o1} (hours)	q ₁ C _{o1} (10 ⁻⁶ kg/s)	q ₁ (10 ⁻⁶ m ³ /s)	C _{o1} (kg/m ³)
1	1440	18	0.23	0.65	0.35
2	1300	18	0.09	0.46	0.20
3	1215	18	0.23	0.50	0.45
4	1200	18	0.09	0.21	0.45
5	1188	18	0.24	0.54	0.45
6	1085	18	0.06	0.18	0.35
7	1048	2	0.27	0.53	0.50
8	918	9	4.2	1.5	2.80
9	843	-24	25.	28.	0.90

K = 5.0 x 10⁻⁴ m²/s
 Q = 3.3 x 10⁻⁵ m³/s



XBL 873-9947

Figure 1. Schematic picture of a wellbore with three inflow points and a well-bore flow rate w from below.

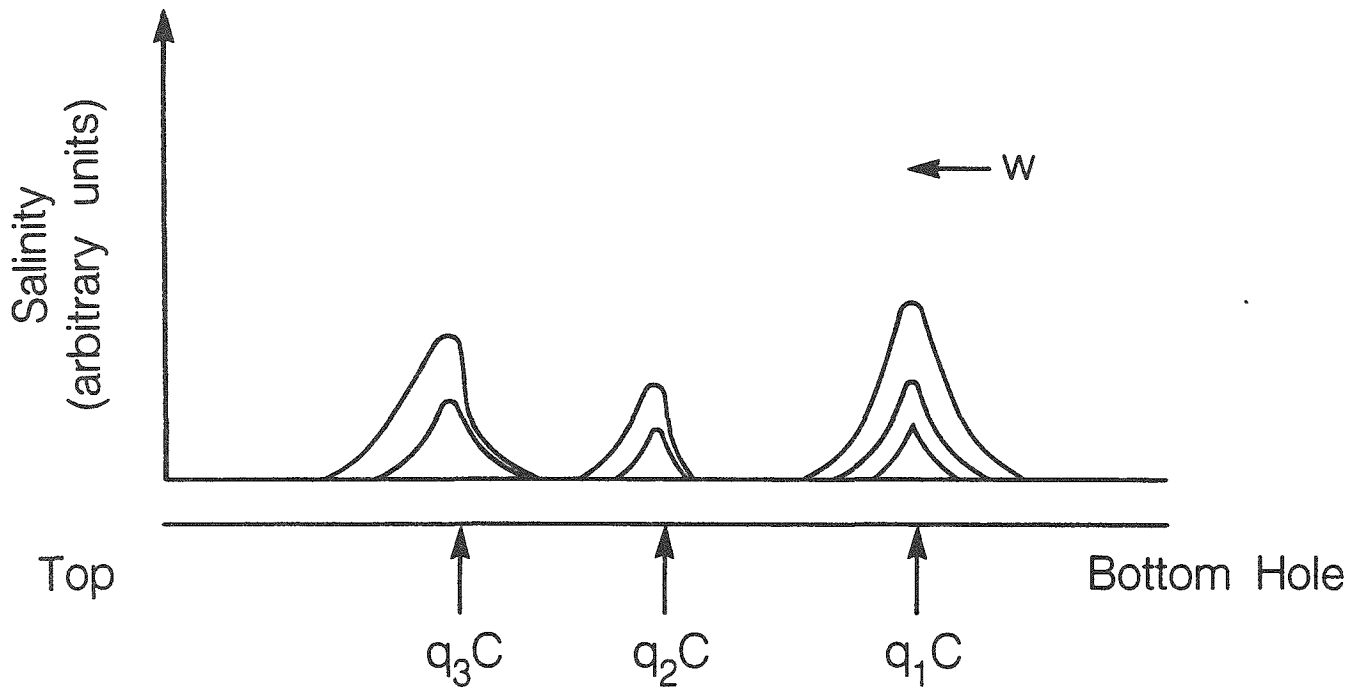
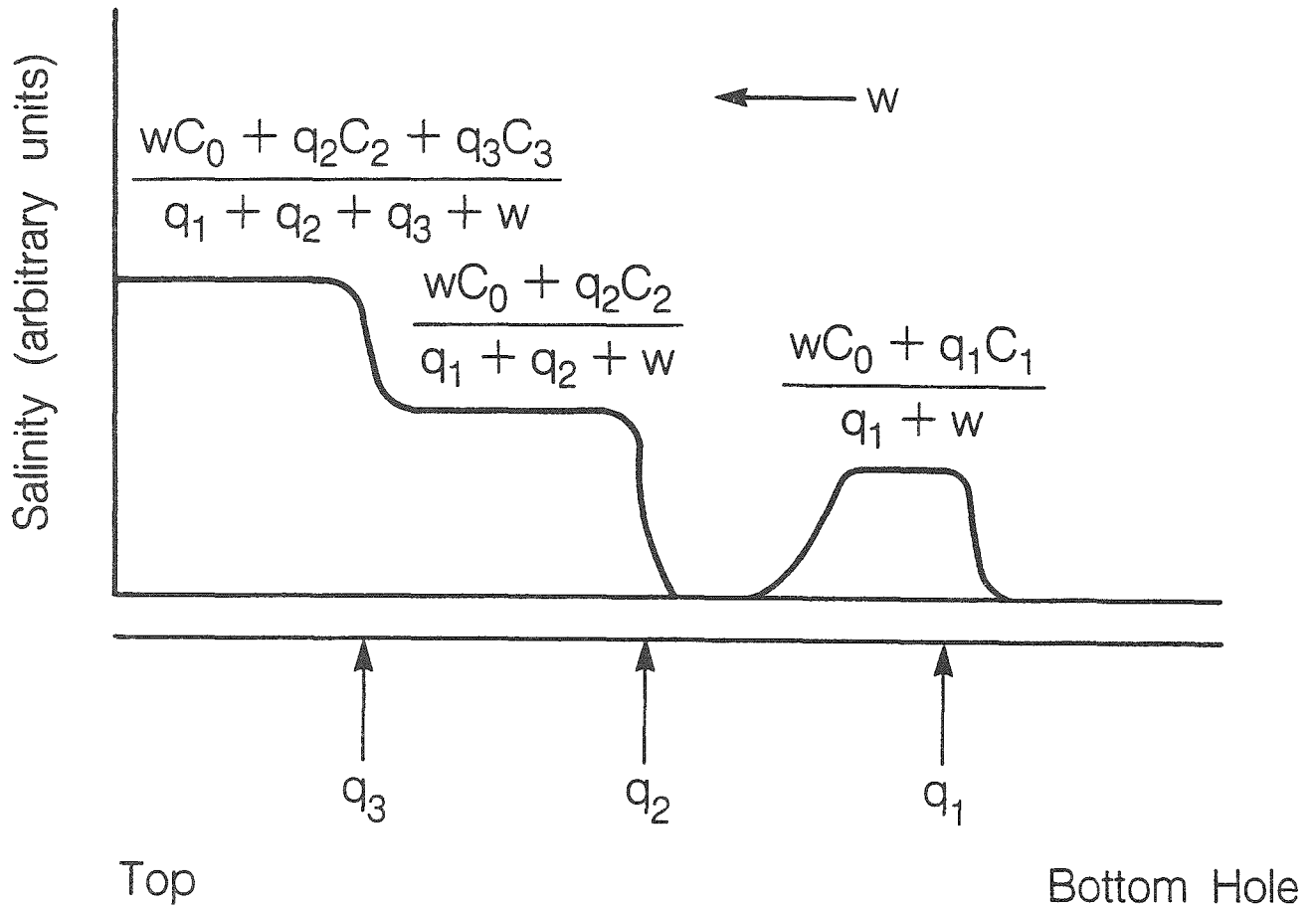
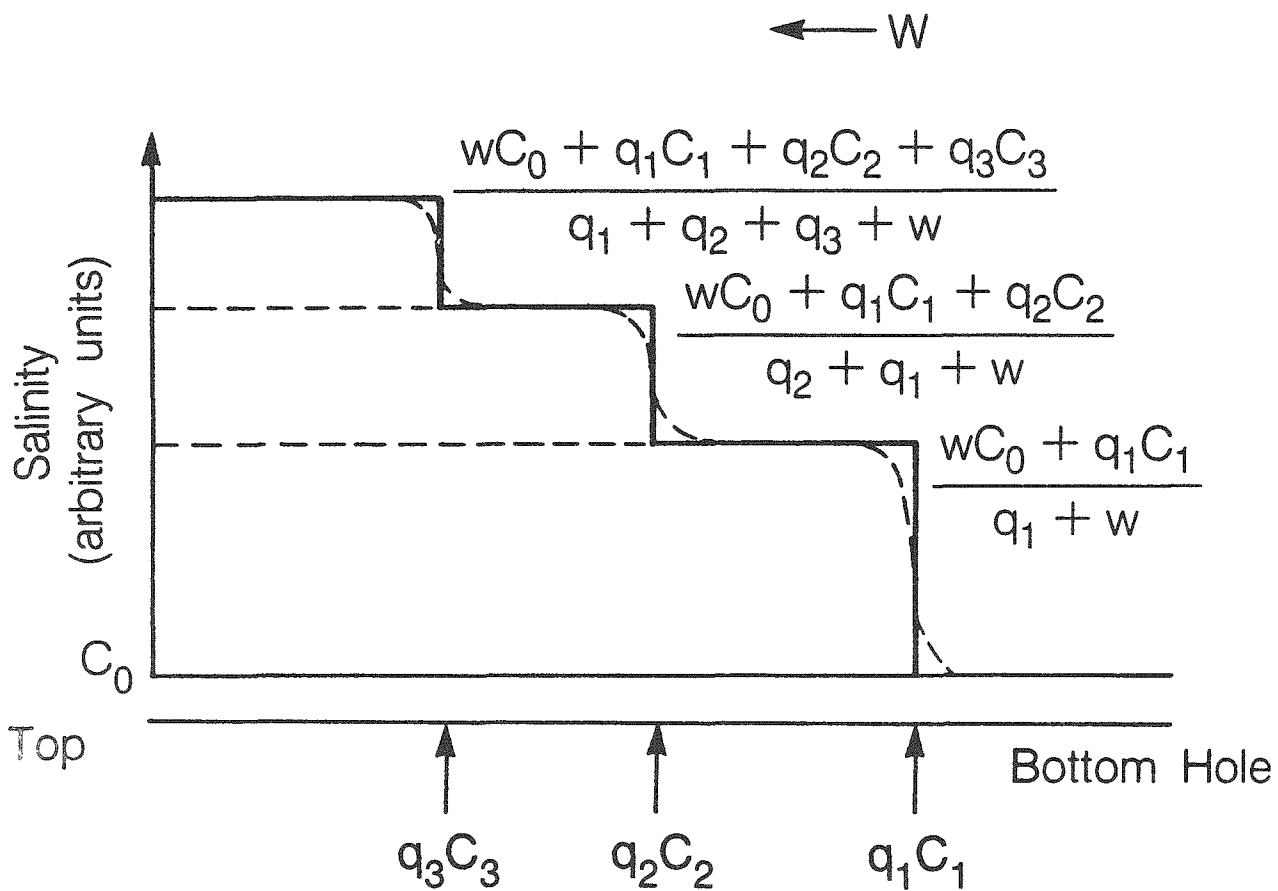


Figure 2. Schematic picture of salinity curves from three inflow points in a wellbore at early times.



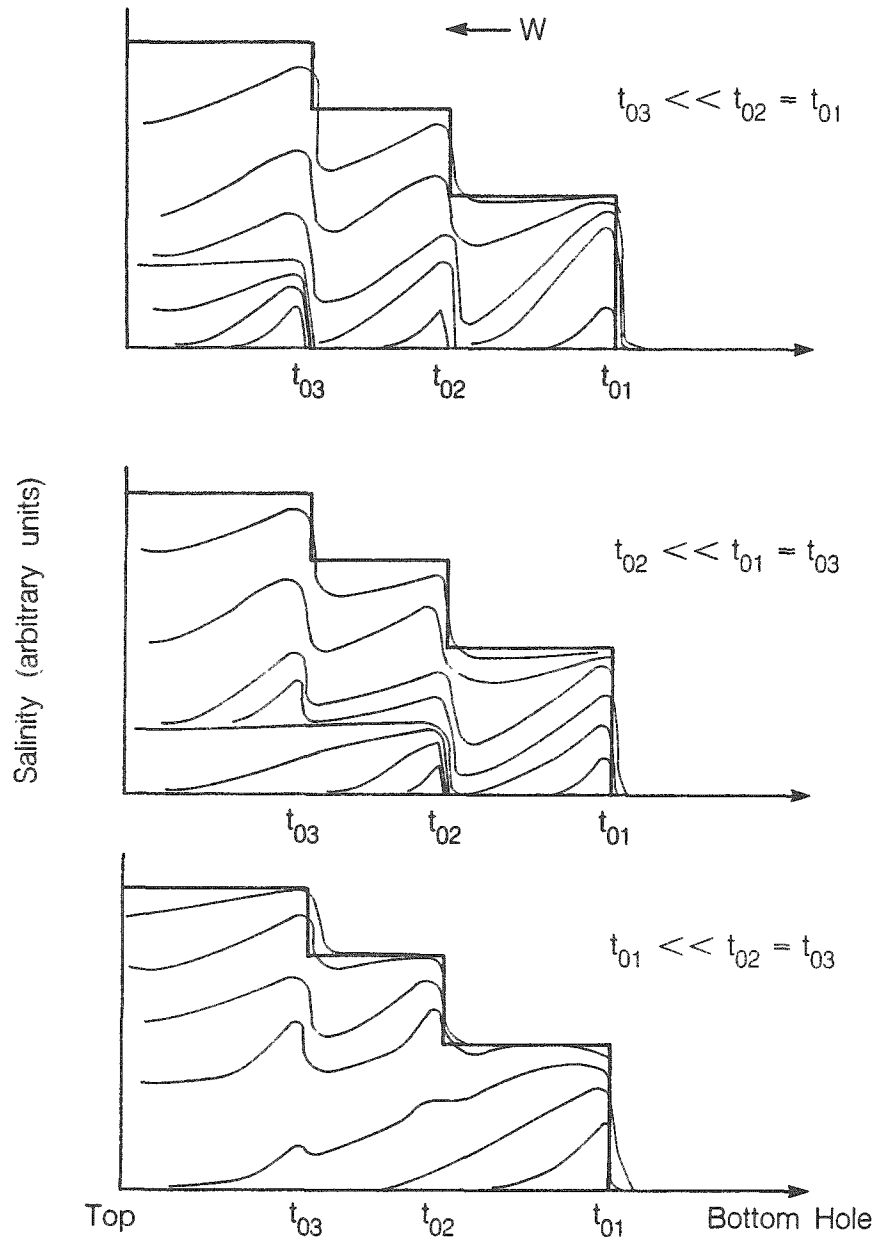
XBL 873-9968

Figure 3. Schematic picture of salinity curves at a large time, assuming very small diffusion effects.



XBL 873-9945

Figure 4. Schematic picture of salinity concentration curves at the very large time limit, assuming very small diffusivity effects.



XBL 873 9946

Figure 5. Schematic picture of salinity concentration curves from early to later times, assuming one of the three inflow points begins much earlier than the other two.

$C(x,t)$ at $t=1, 4, 9, 16$ sec

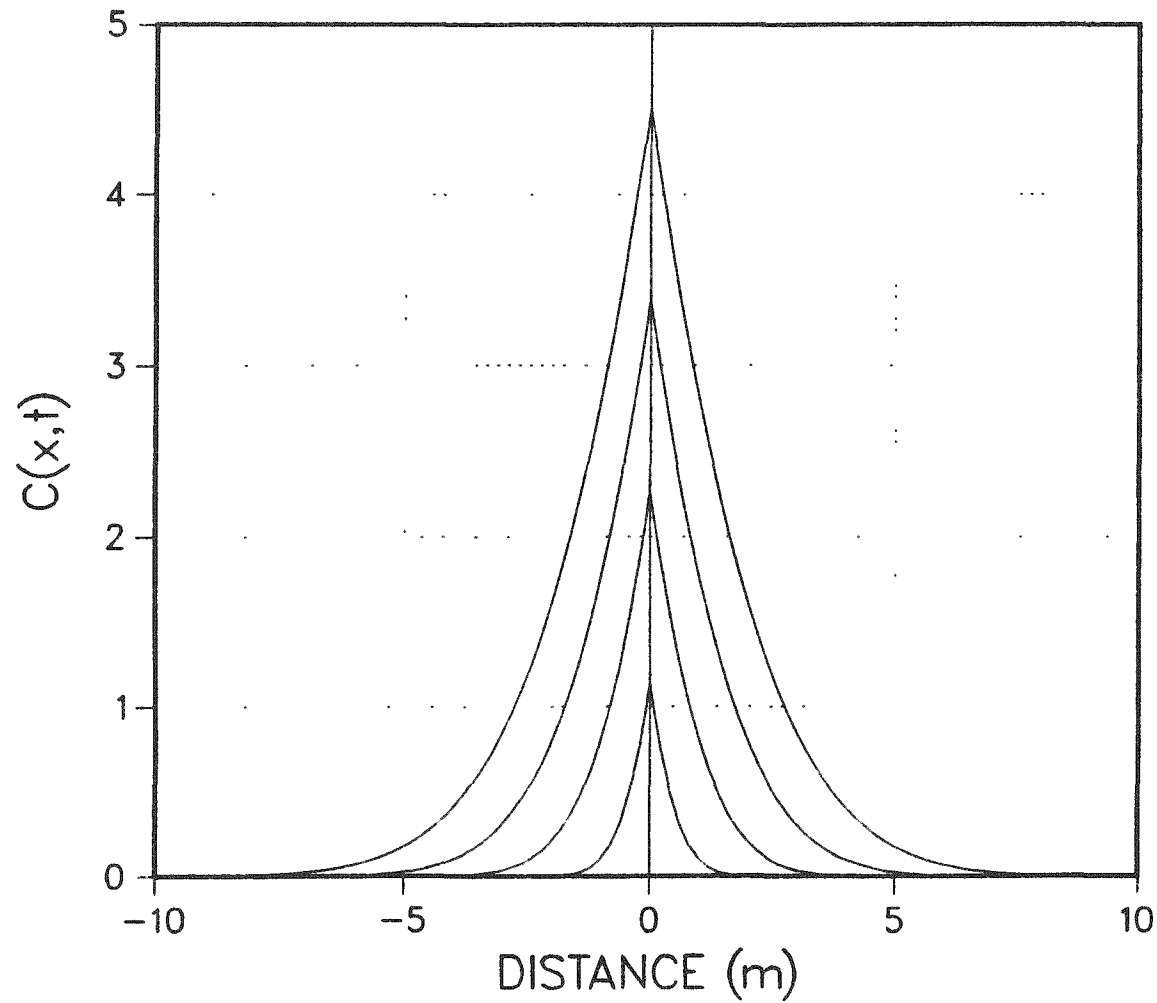


Figure 6. Analytic results for one inflow point for early times.

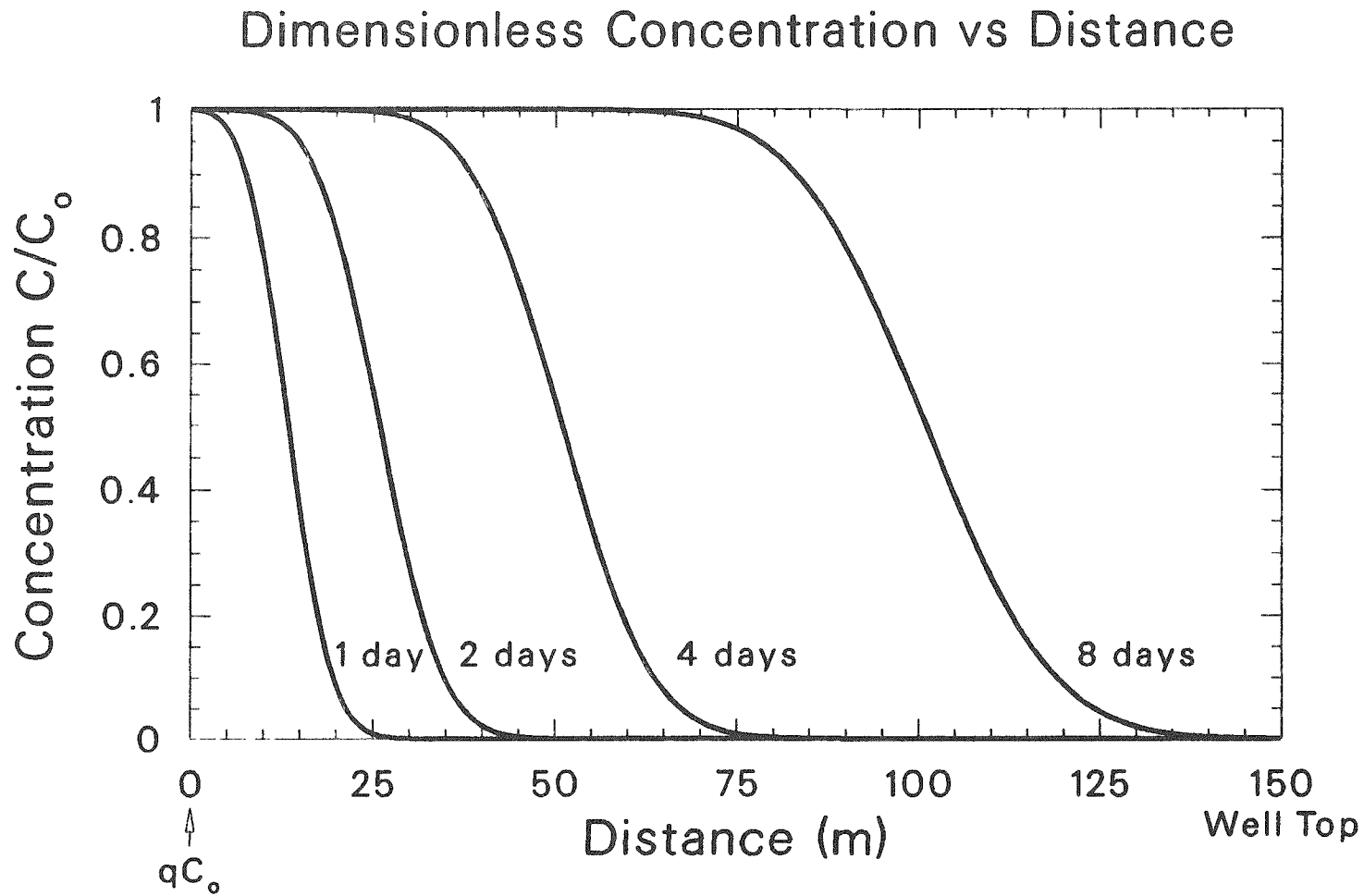
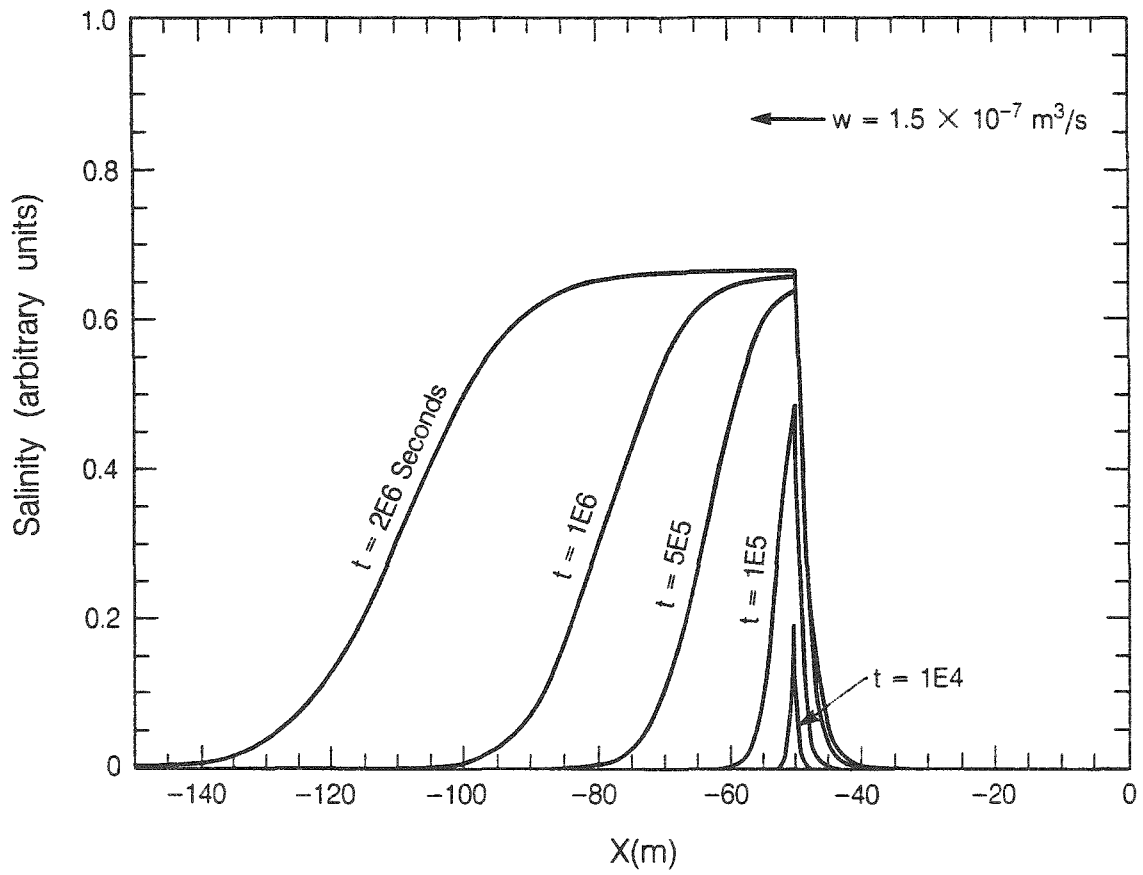
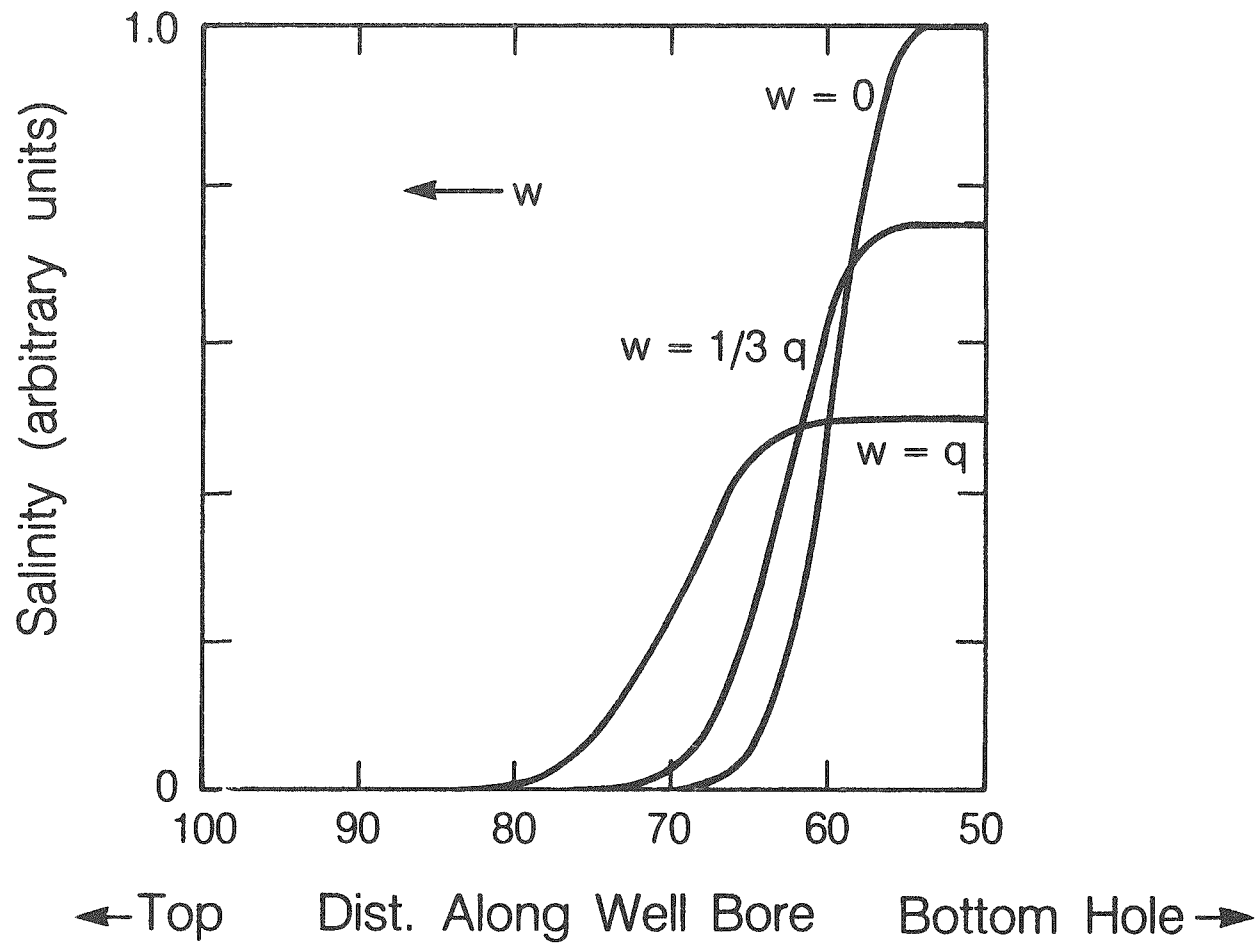


Figure 7. Analytic results for one inflow point for later times.



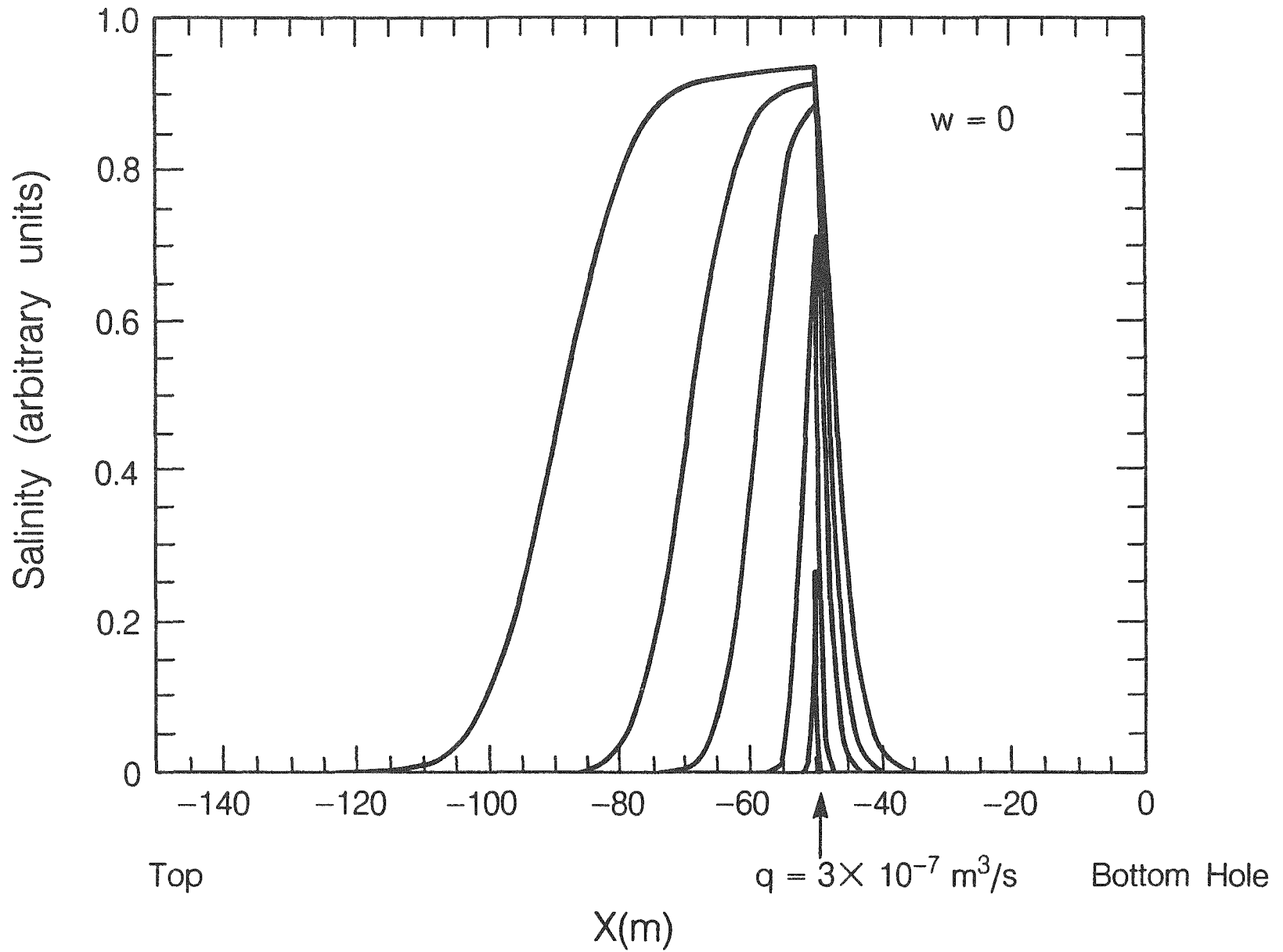
XBL 873-9953

Figure 8. Numerical results for one inflow point from early to later times.



XBL 873-9948

Figure 9. Numerical results for one inflow point at flowrate q for three wellbore flow rate from below at $w = 0$, $w = 1/3q$ and $w = q$.



XBL 873-9952

Figure 10a. Numerical results for one inflow point and $w = 0$ for dispersion constant K equal to $25 \text{ m}^2/\text{s}$.

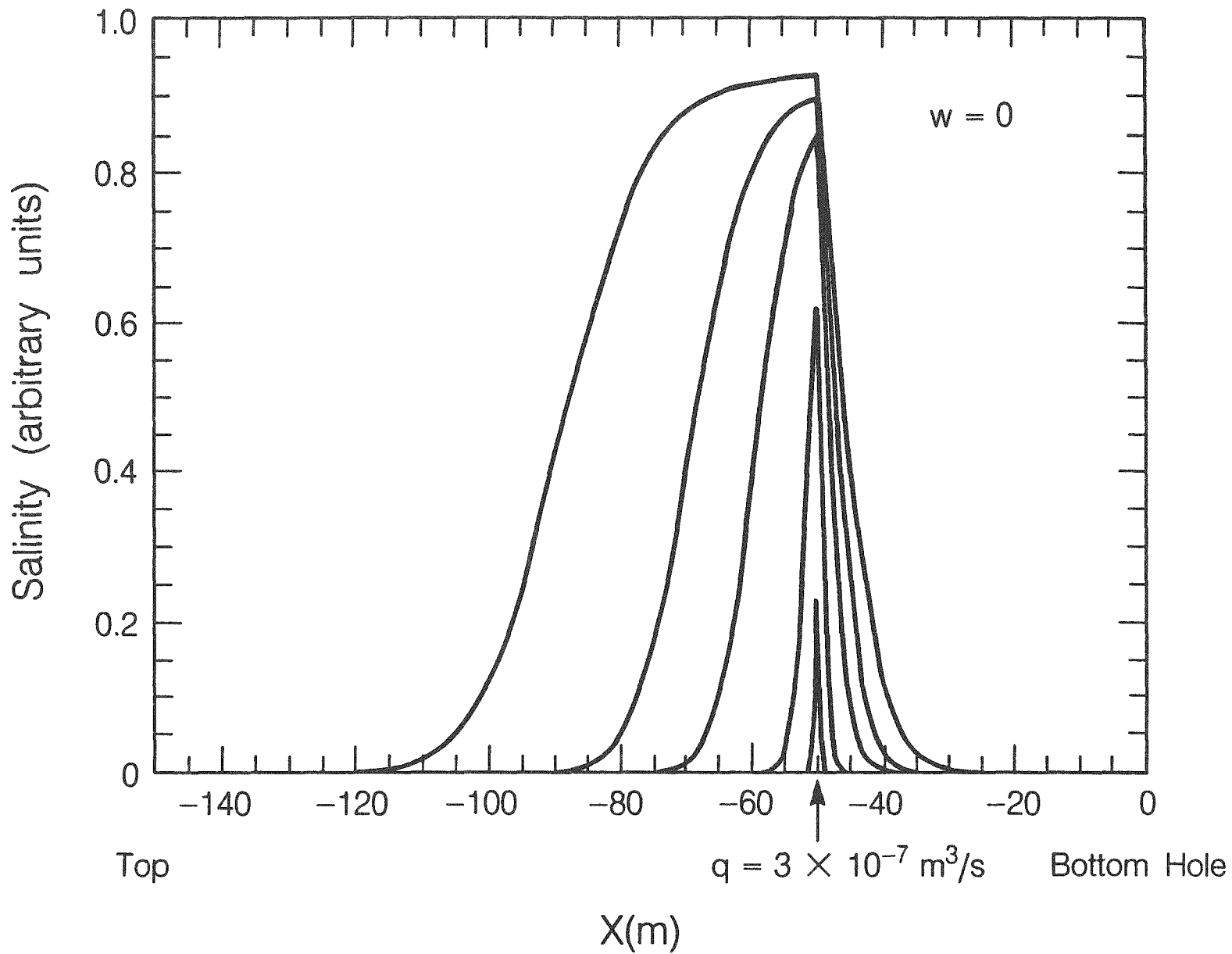
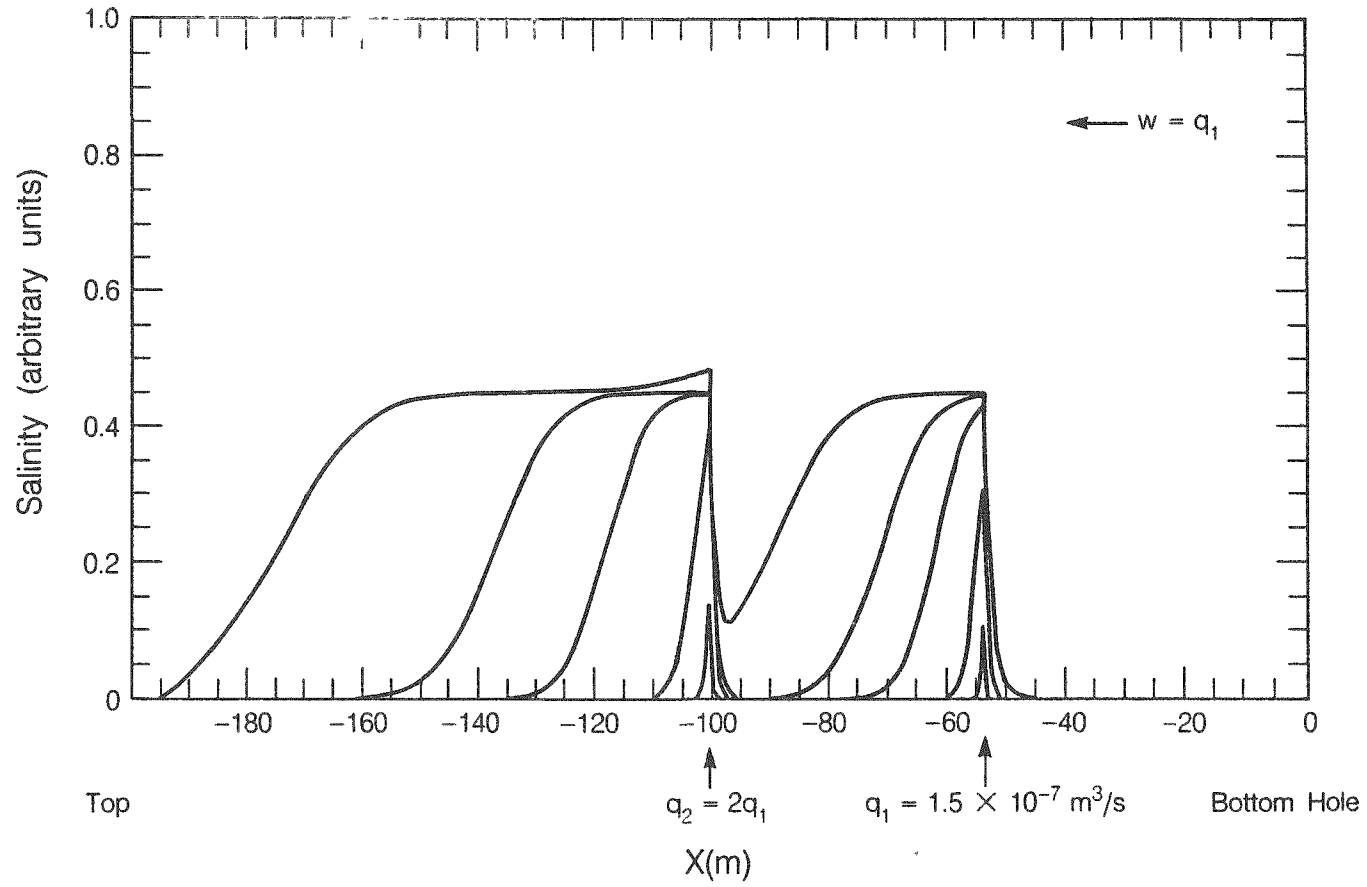
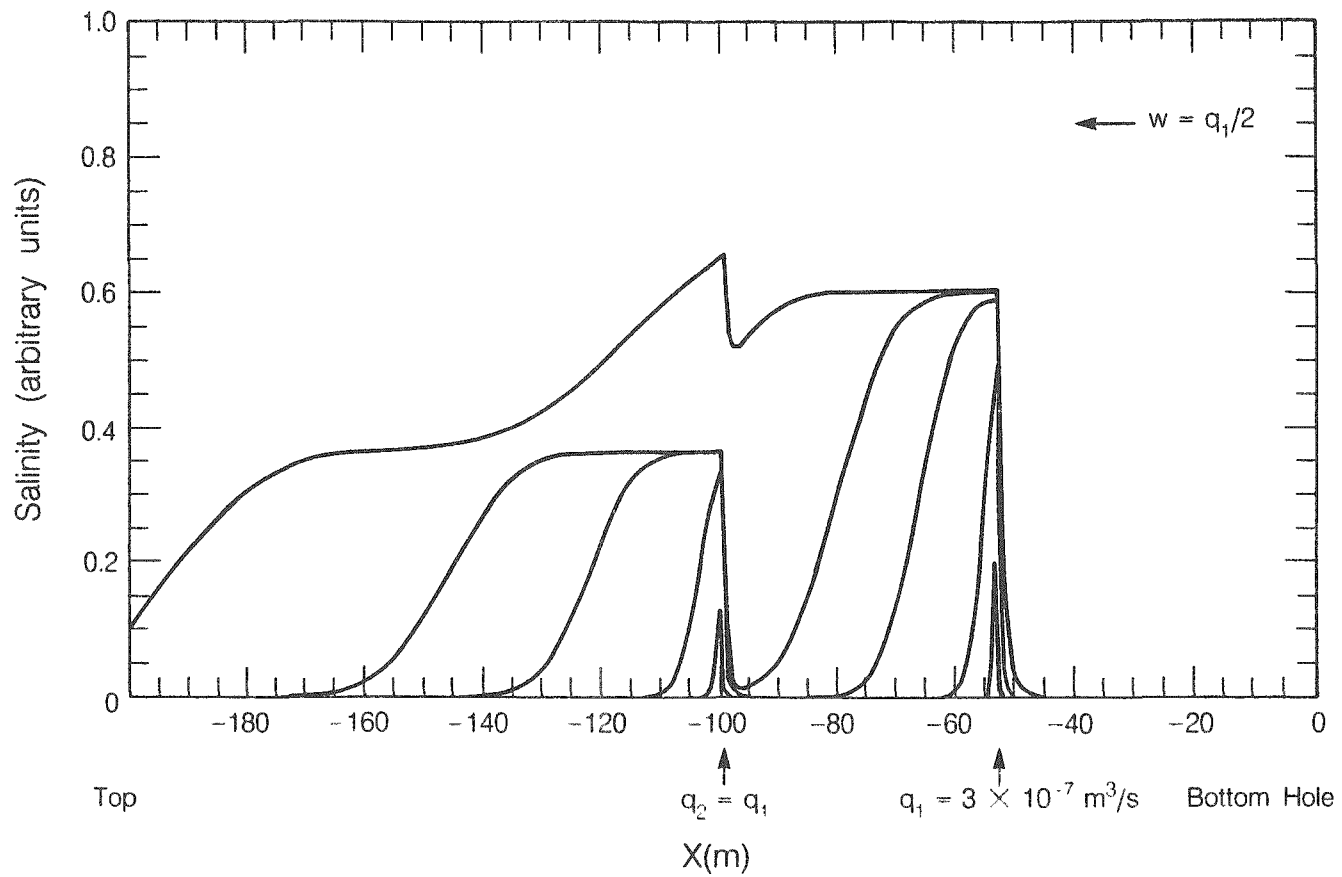


Figure 10b. Numerical results for one inflow point and $w = 0$ for dispersion constant K equal to $50 \text{ m}^2/\text{s}$. XBL 873-9951



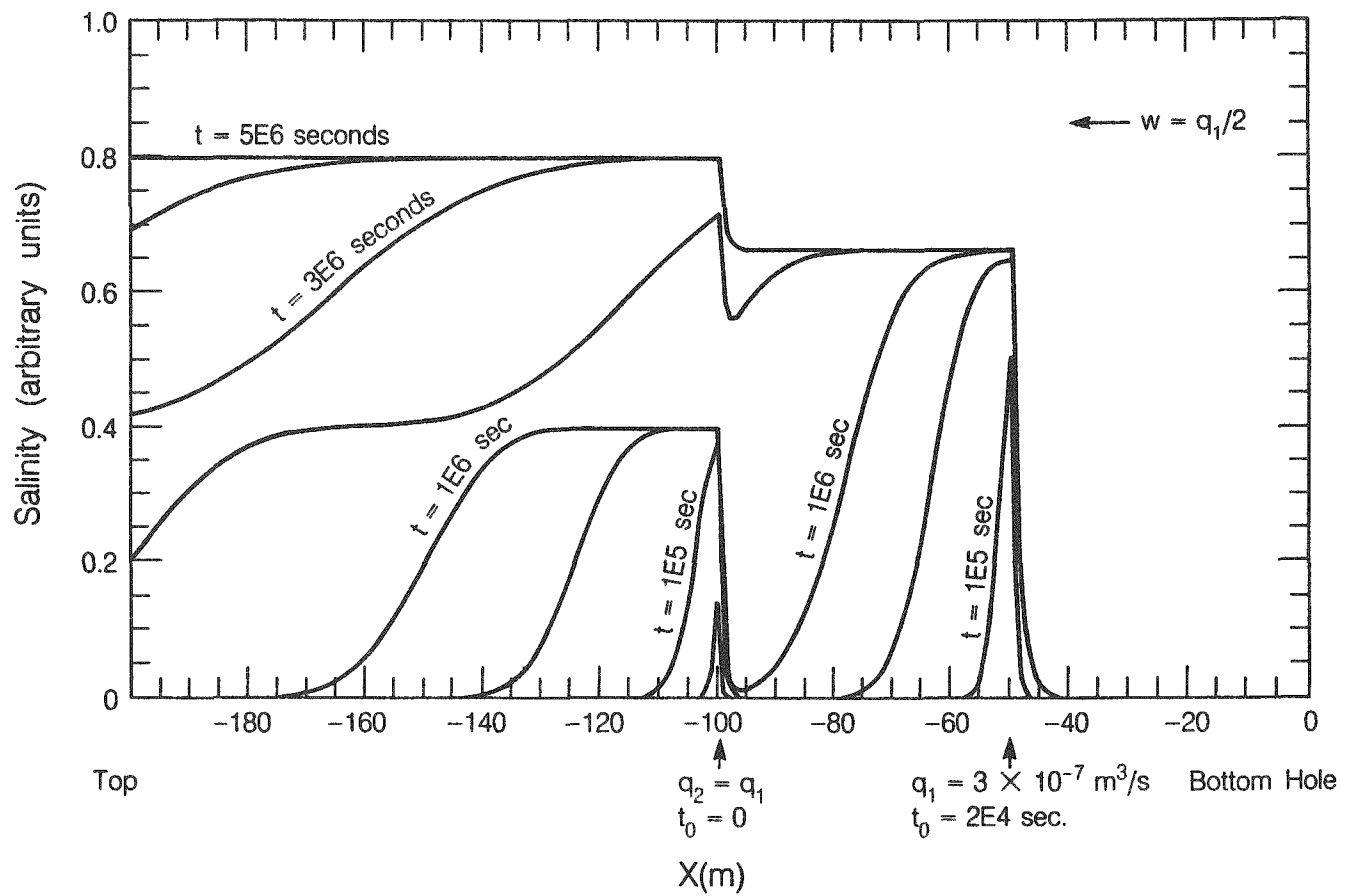
XBL 873 9954

Figure 11. Numerical results for two inflow points.



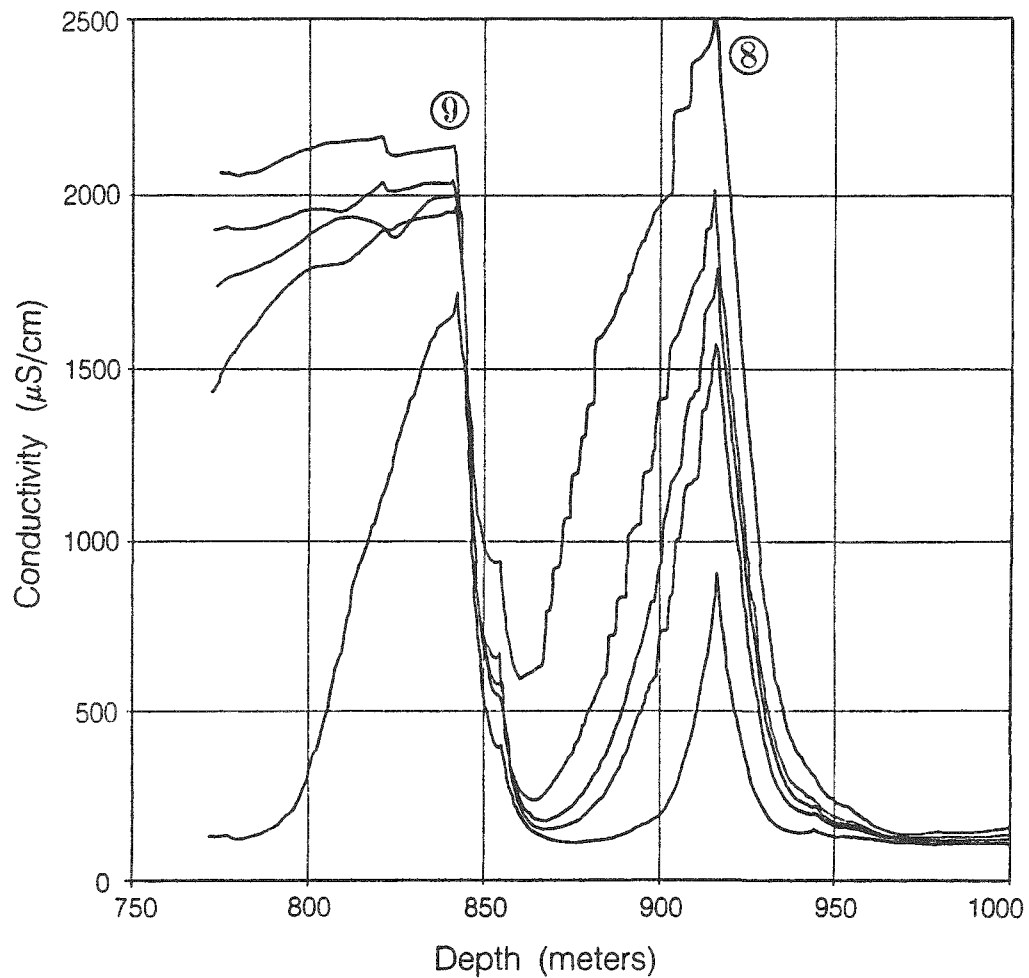
XPL 873 9955

Figure 12. Numerical results for two inflow points, displaying interference.



XBL 873 9953

Figure 13. Numerical results for two inflow points for large time limit.



XBl. 873 9966

Figure 14. Field fluid-conductivity log data from NAGRA (1986) for the 770-1000 m section of a 1690-m borehole.

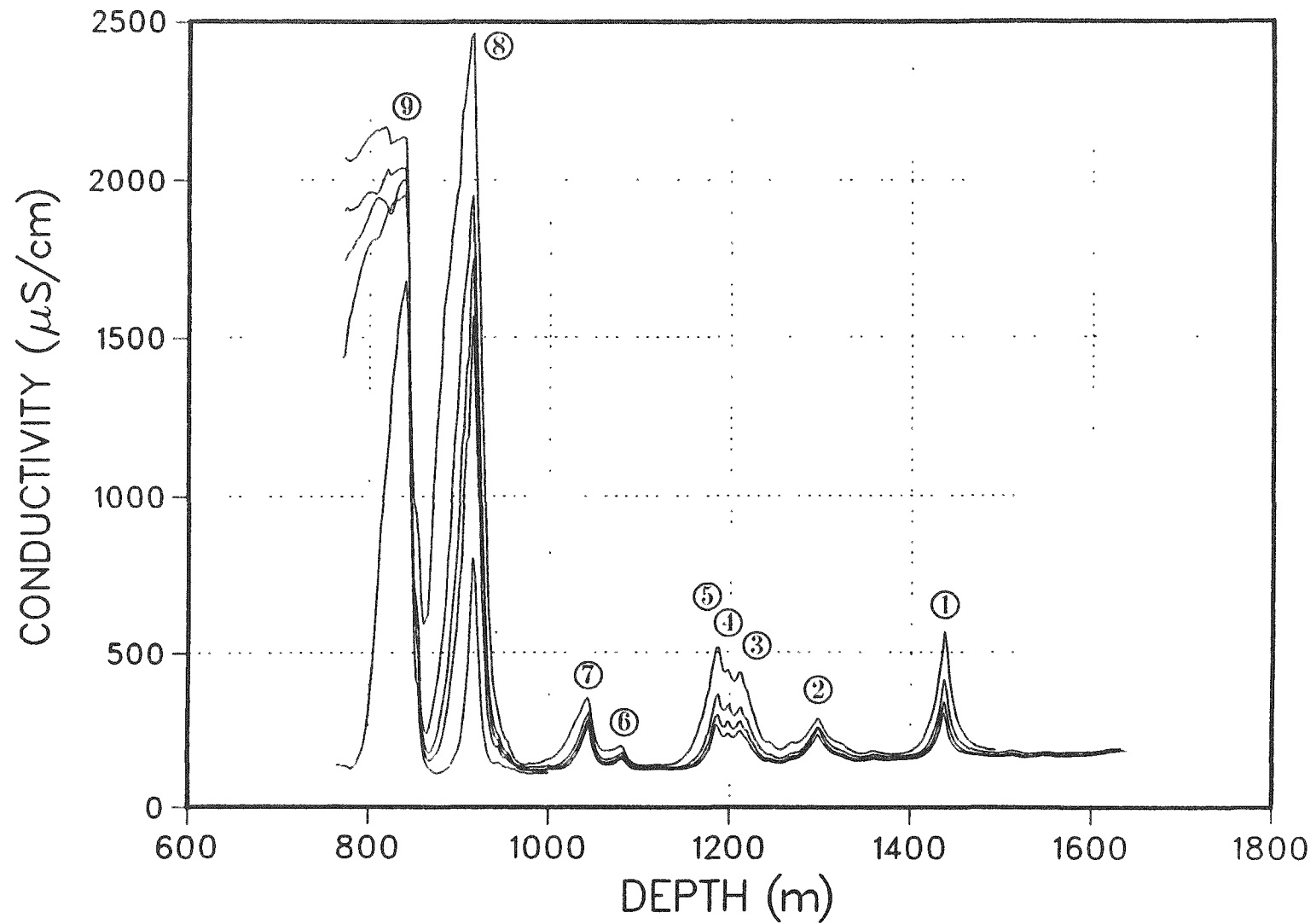


Figure 15. Field fluid-conductivity log data from NAGRA (1986) for the full logged 770-1640 m section of a 1690-m borehole.

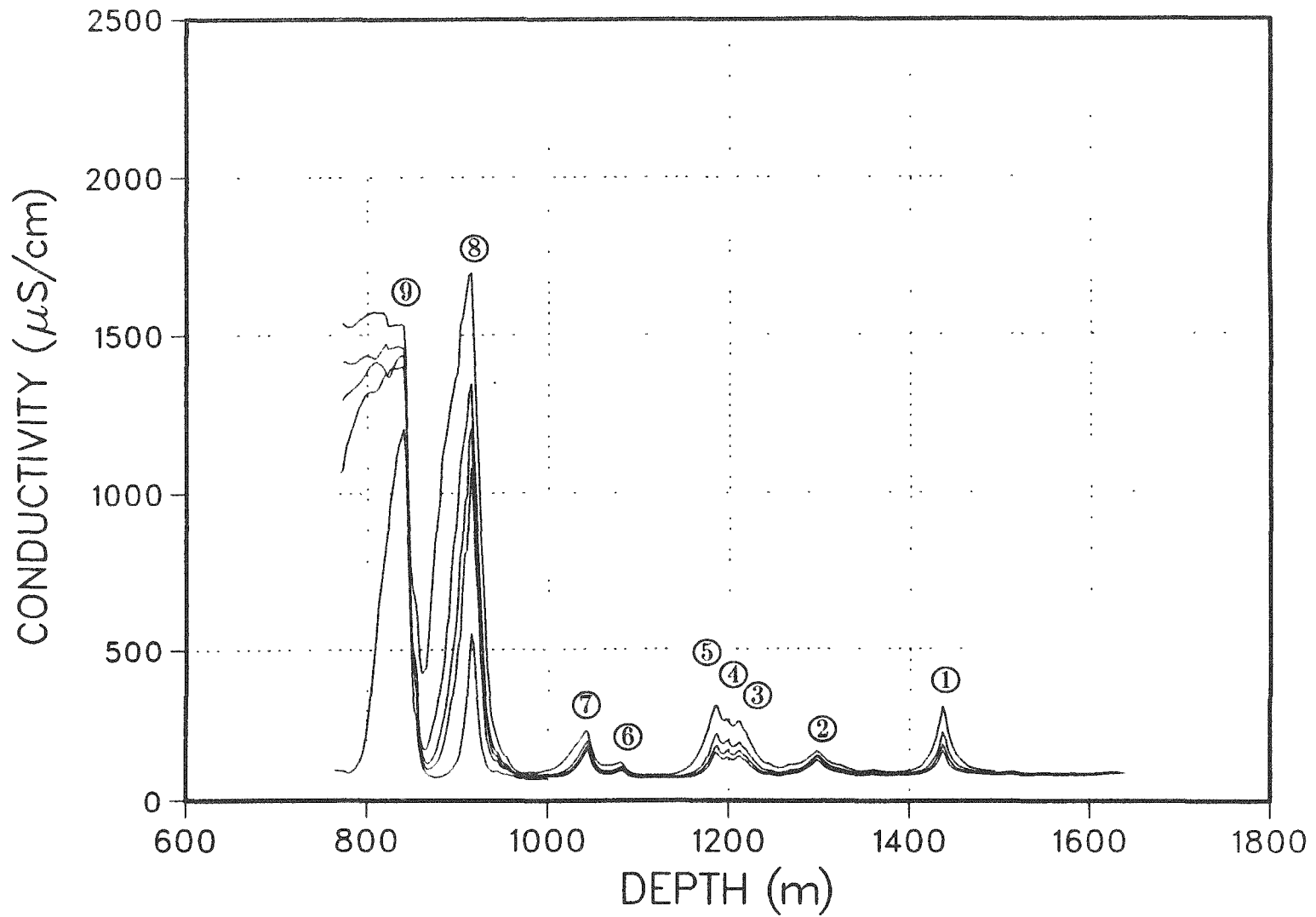


Figure 16. Normalized fluid-conductivity log data.

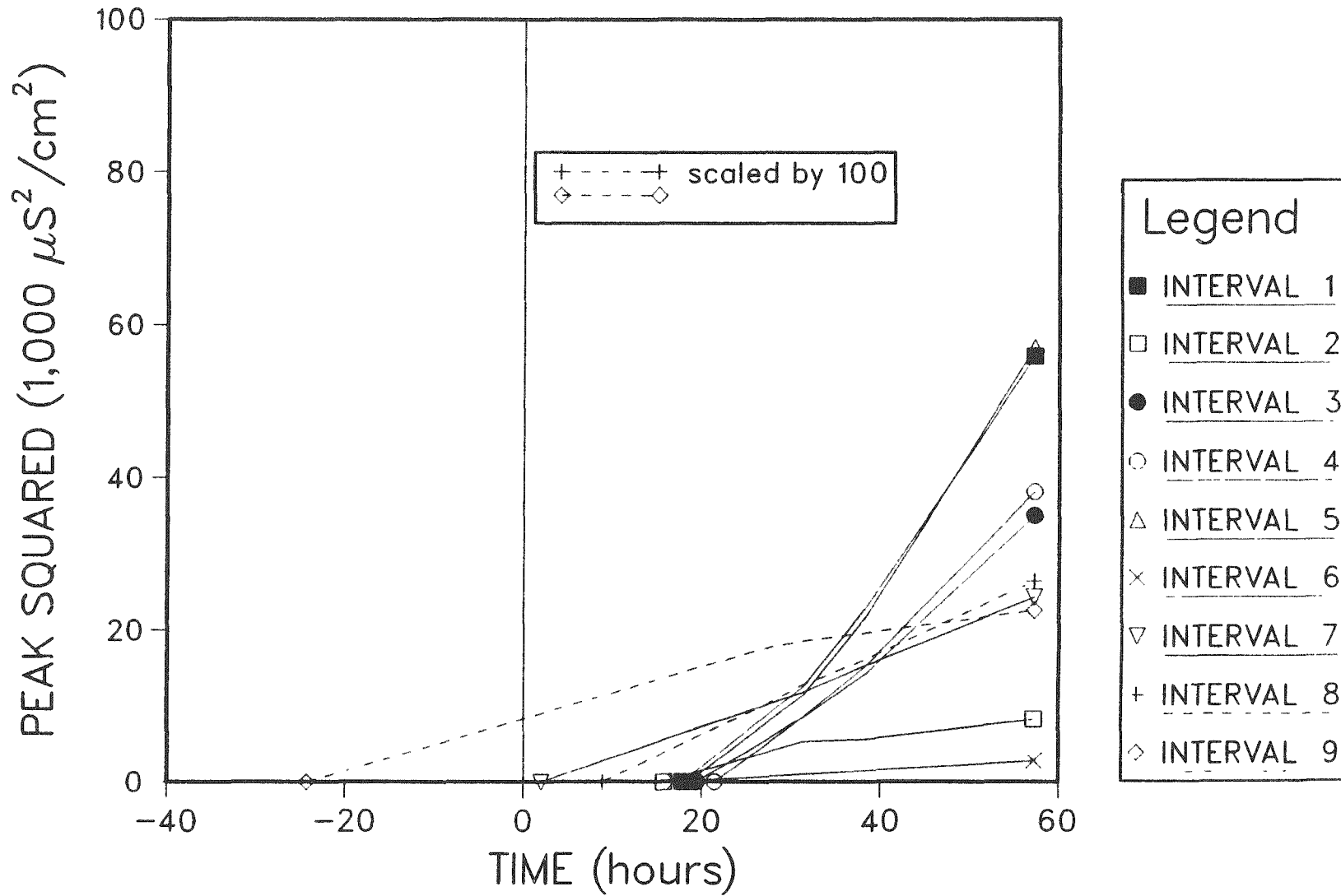


Figure 17. Peak values squared versus time plots for all nine inflow points.

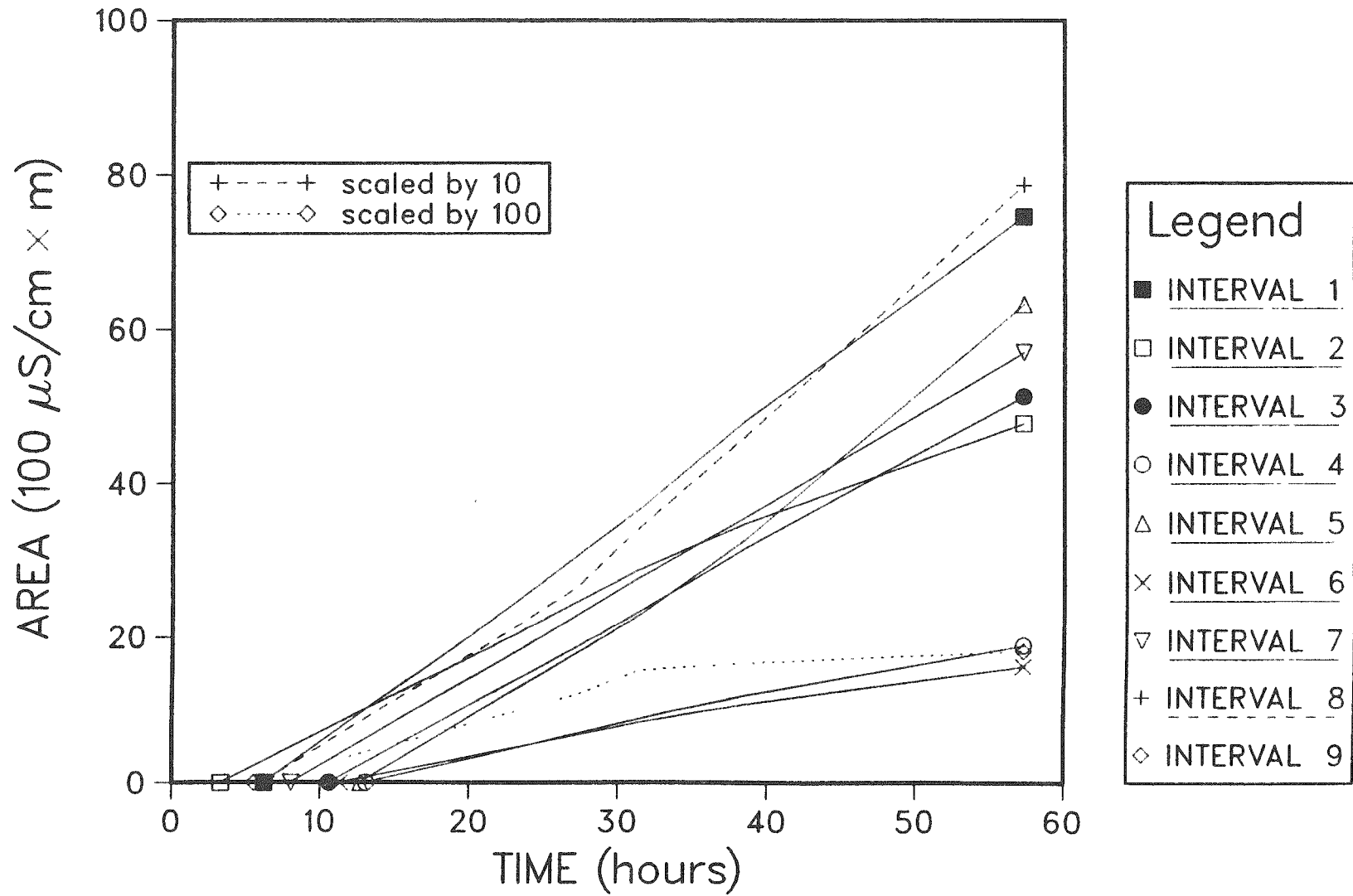


Figure 18. Area versus time plots for all nine inflow points.

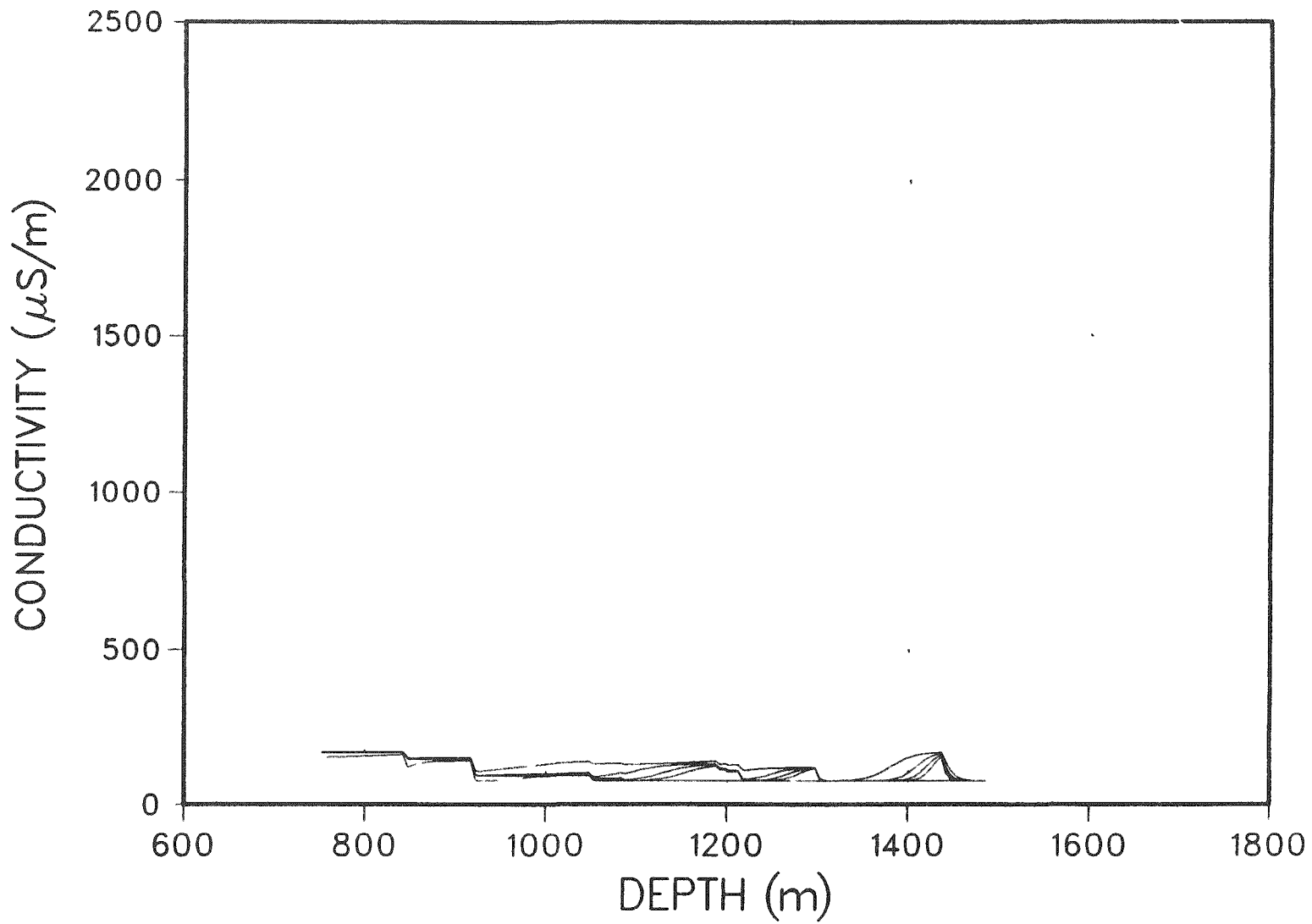


Figure 19. An early attempt to match the field data. The parameters used are given in Table 3. The assumed total flowrate from the borehole section under study was too large.

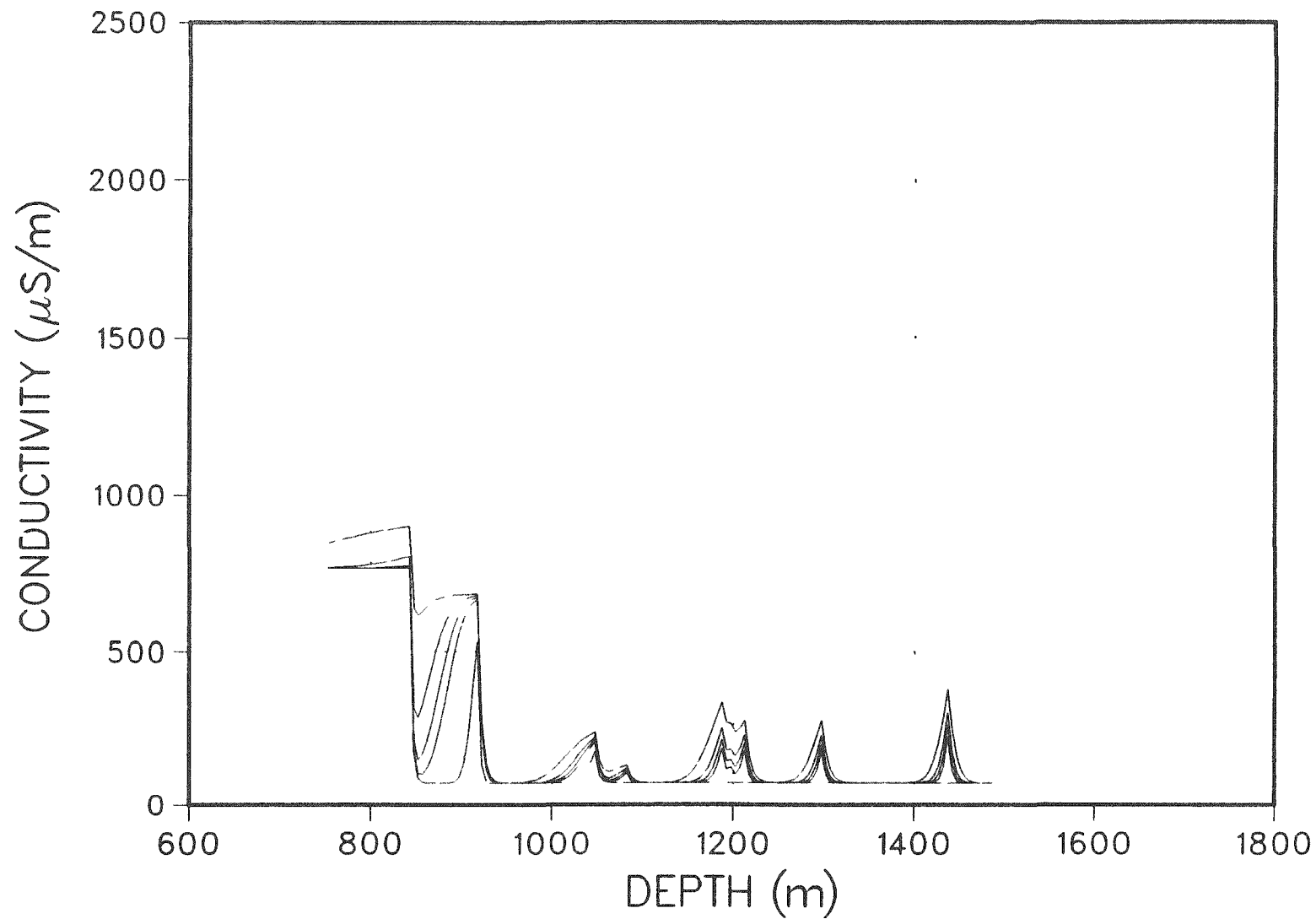


Figure 20. A base case for sensitivity studies. The parameters used are given in Table 4. The curves are for time of 13.03, 27.12, 31.38, 38.41 and 57.24.

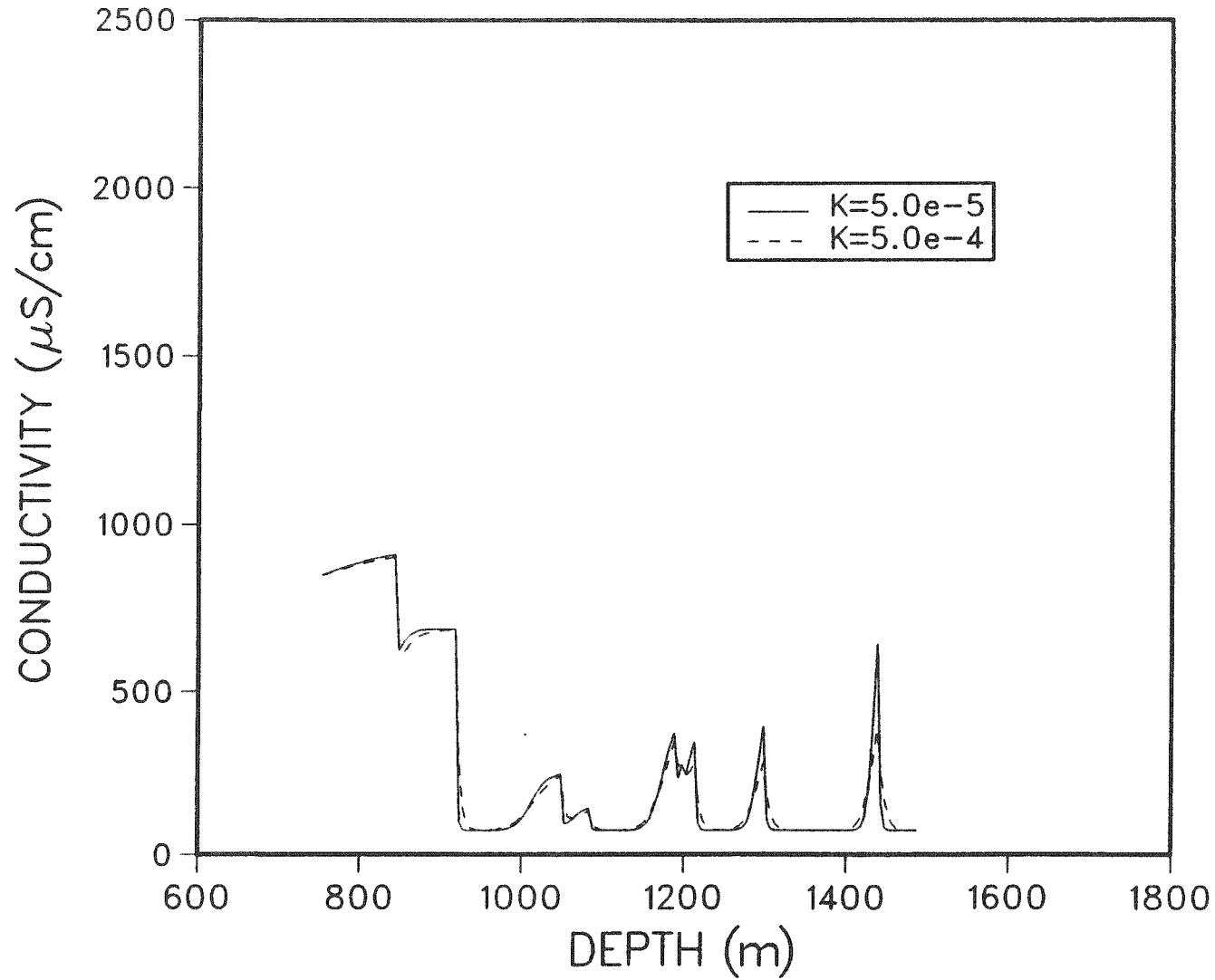


Figure 21. Results if the borehole dispersion coefficient is reduced by a factor of 10 relative to the base case, the other parameters remaining the same. Only results for 57.24 hours are shown. The broken curve is the base case results.

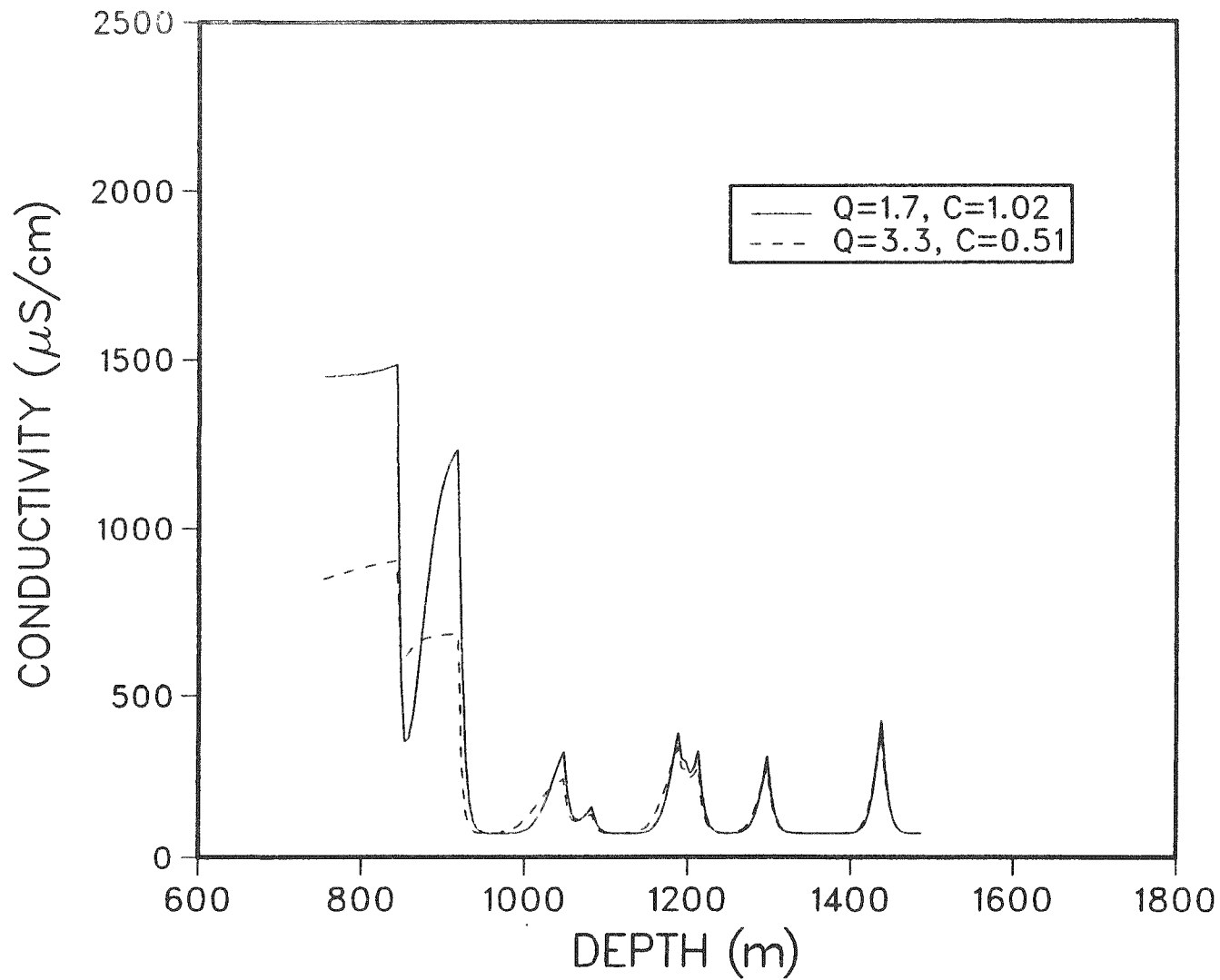


Figure 22. Results at 57.24 hours of sensitivity studies relative to the base case: In the parameters given in Table 3 $q_i C_{oi}$ are kept the same, but all Q_i' s are increased by a factor of 2 and all C_{oi}' s are decreased by a factor of 2.

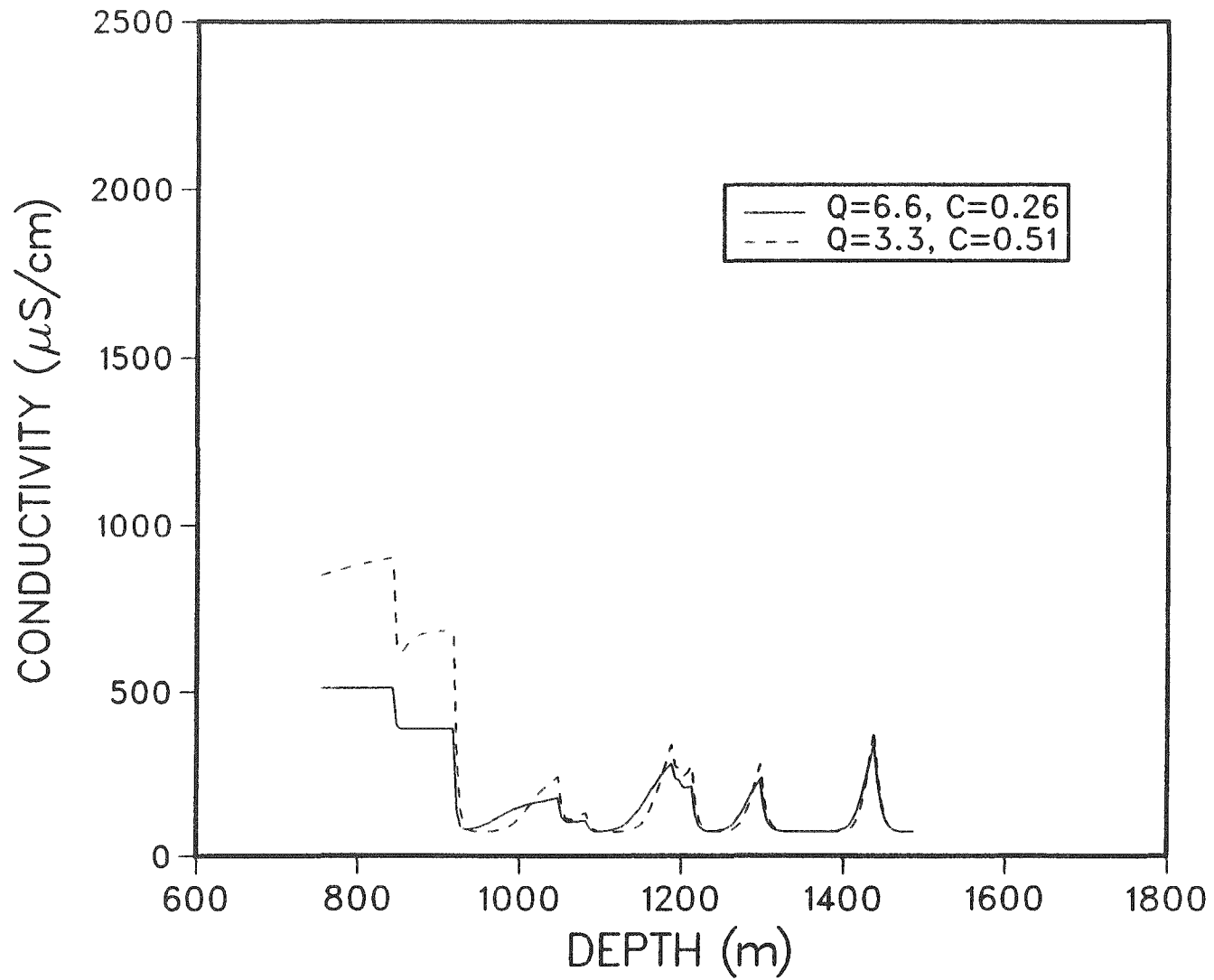


Figure 23. Results at 57.24 hours of sensitivity studies relative to the base case: In the parameters given in Table 3 $q_i C_{oi}$ are kept the same, but all C_{oi}' s are increased by a factor of 2 and all q_i' s are decreased by a factor of 2.

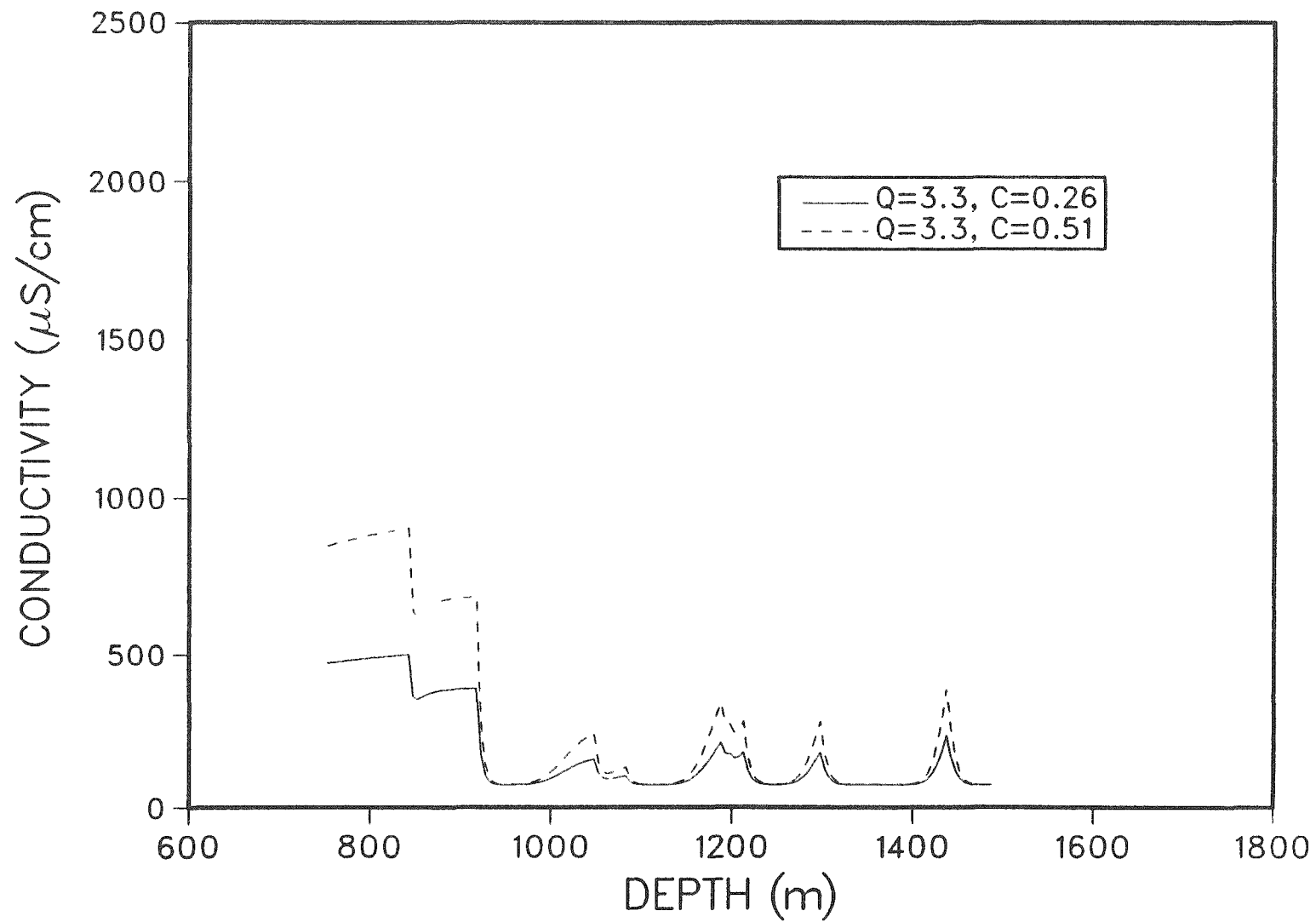


Figure 24. Results at 57.24 hours of sensitivity studies relative to the base case: In the parameters given in Table 3 $q_i C_{oi}$ are kept constant, but all C_{oi} and $q_{oi} C'_{oi}$ are reduced by a factor of 2.

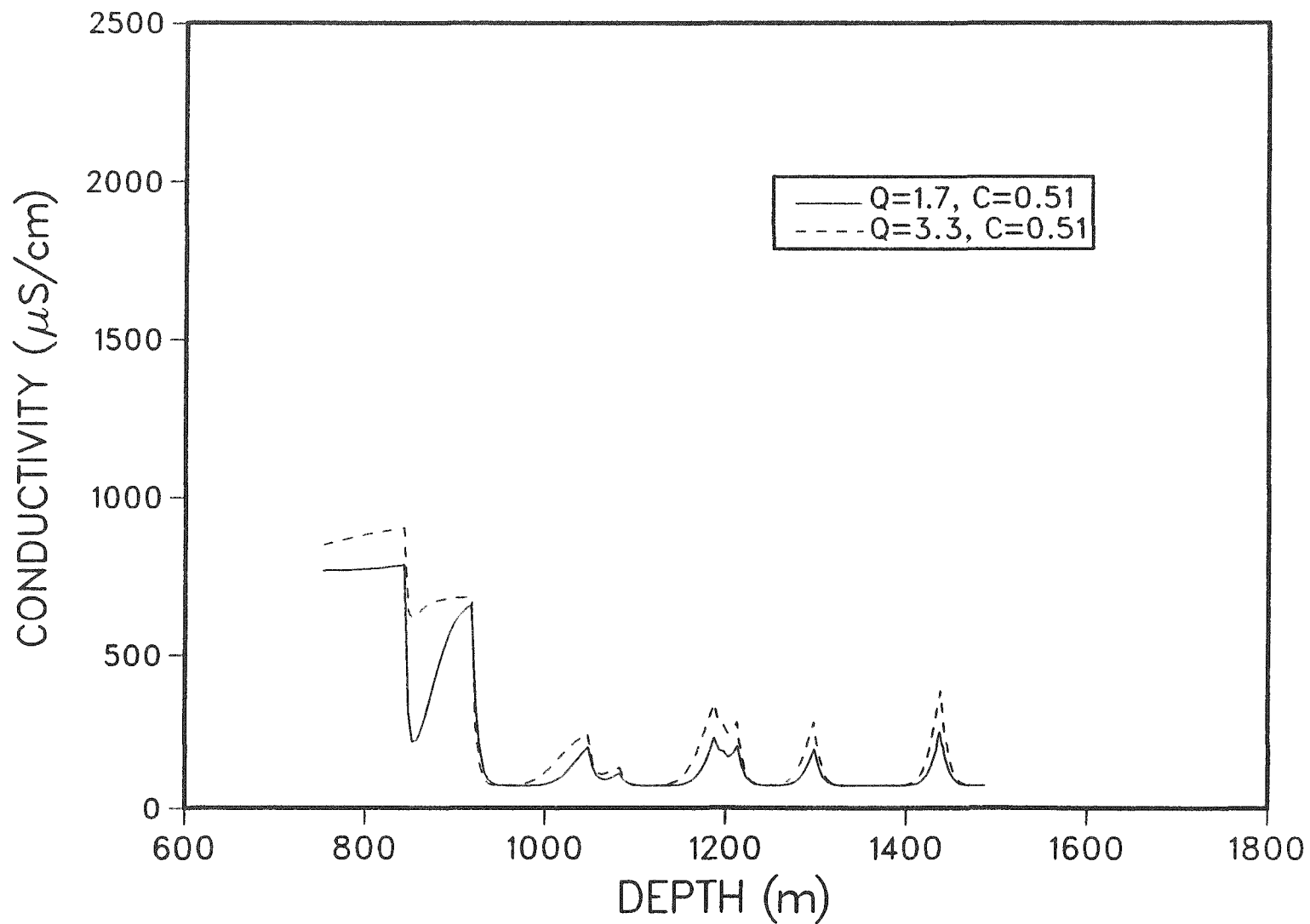


Figure 25. Results at 57.24 hours of sensitivity studies relative to the base case: In the parameters given in Table 3 all C_{oi}' s are kept constant, but all q_i and C_{oi} are reduced by a factor of 2.

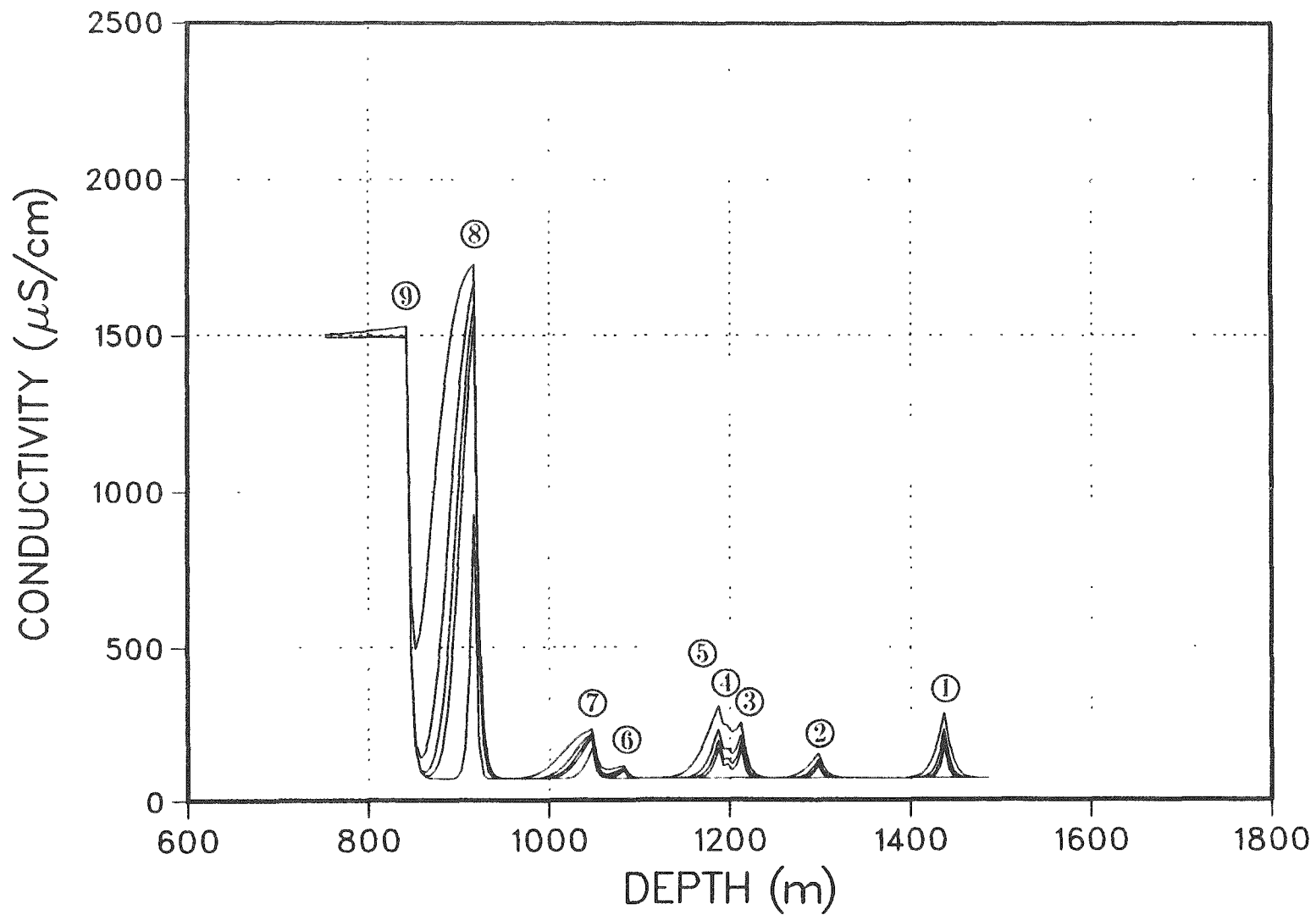


Figure 26. The final match to field data with the parameters given in Table 4, for times = 13.03, 27.12, 31.78, 38.41 and 57.24 hours.

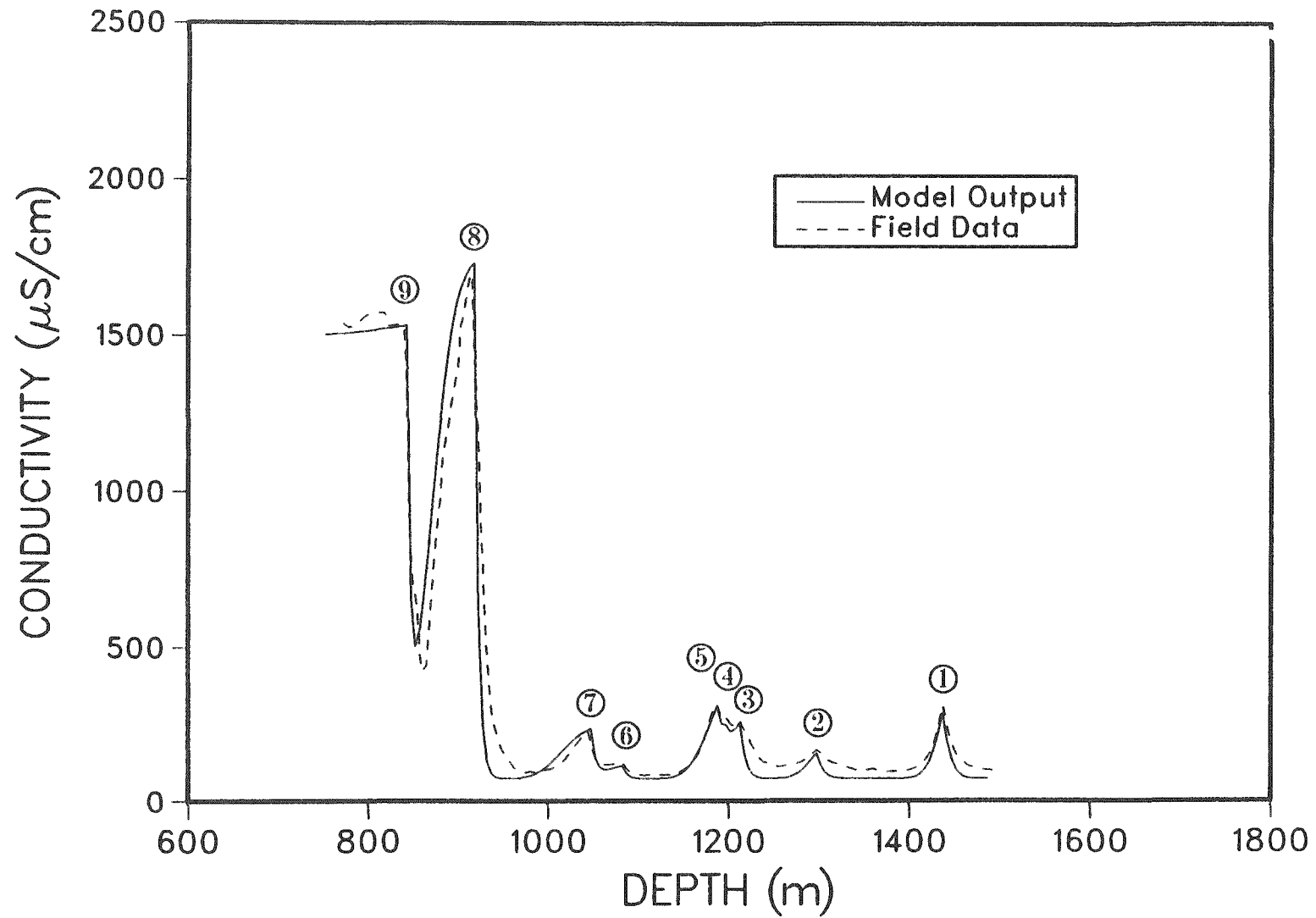


Figure 27. Comparison of field data (dashed lines) and final-matched calculated results (solid lines). Only results at 57.24 hours are shown.

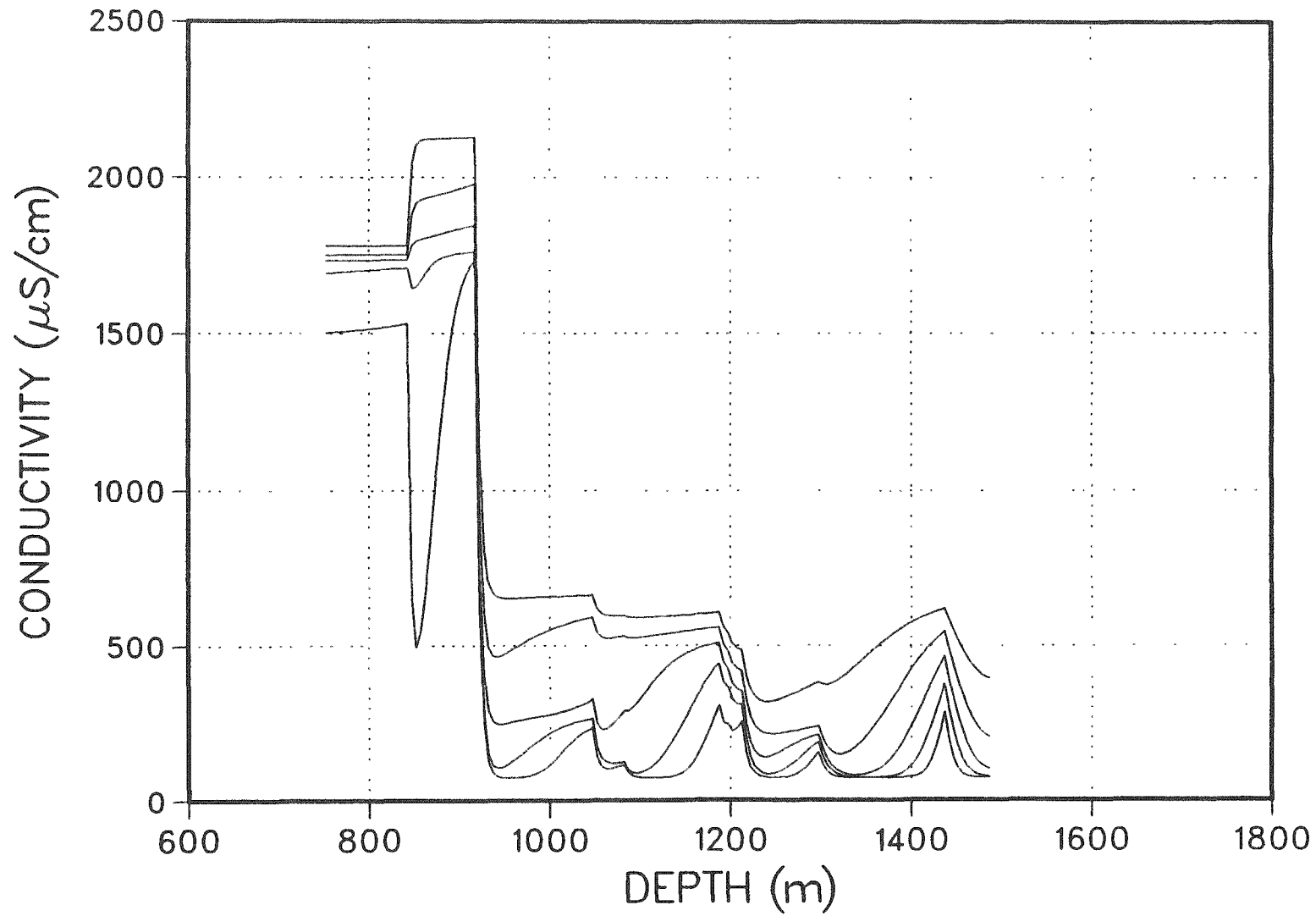


Figure 28. Calculated results at large times (57, 115, 230, 460, 918 hours) based on the final-match parameters given in Table 4.